Maria Leonor Joaquim do Nascimento Matias

Bachelor in Engineering of Micro and Nanotecnologies

Paper-based nanoplatforms for multifunctional applications

Dissertation to obtain the Master Degree in

Engineering of Micro and Nanotecnologies

Advisor: Daniela da Silva Nunes Gomes, Assistant professor,
Faculty of Sciences and Technology, NOVA University of Lisbon

Co-advisor: Ana Cláudia Madeira Botas Gomes Pimentel, Post-Doc,
Faculty of Sciences and Technology, NOVA University of Lisbon

Examination Committee:

Chairperson: Dr. Rodrigo Ferrão de Paiva Martins

Raporteur: Dr. Susana Isabel dos Santos Silva Sério Venceslau

Member: Dr. Daniela da Silva Nunes Gomes

FACULDADE DE CIÊNCIAS E TECNOLOGIA
UNIVERSIDADE NOVA DE LISBOA

September, 2018

Paper-based nanoplatforms for multifunctional applications

“Για να πετύχεις, πρέπει πρώτα να πιστέψεις ότι μπορείς.”

Νίκος Καζαντζάκης

(“Para teres sucesso, deves primeiro acreditar que consegues.”)

Níkos Kazandzákis

Acknowledgements

Firstly, I would like to thank my supervisor, Dr. Daniela Gomes for all the support, availability, encouragement and useful advice on my research during these six months. Without her advice the article would not be possible. I am sincerely grateful to her who steered me in the right direction, whenever she thought I needed it.

Another important person was Dr. Ana Pimentel, who supervised my work in the lab giving me helpful suggestions. Also, thank you engineer Raquel Borda D'Água for the help in the antibacterial assays and the important tips. She helped me how to be more organized and that even if I had not achieved good results, the most important thing was to be able to justify them and not stress out. Additionally, thank you Prof. Maria Paula Duarte for the help with the antibacterial assays in the Department of Science and Technology of Biomass.

I would also like to thank engineer Sofia Ferreira for helping me with UV sensors, ZnO seed layers and assisting me in finding better alternatives when experiments did not work out. Some of my measurements with the UV would not be possible without engineers Andreea Panaiate and Ana Filipa from Romania. We had such a good communication in the lab that the schedule with the microwaves and the UV-VIS spectrophotometer worked really well. I wish them a huge success with their future work and maybe one day we will meet each other again.

I would also like to thank Prof. Elvira Fortunato and Prof. Rodrigo Martins, not only for the opportunity to work in this prestigious scientific research center: CENIMAT, but also for the access to all the materials/reagents and installations when needed and for their support in my article.

Special thanks to engineer Sónia Pereira for the XRD measurements, to engineer Alexandra for the fast delivery of materials/reagents, to engineer Inês Cunha for showing me the basics in screen-printing, to engineer Tiago Carvalho for showing me the production of ZnO nanorods without seed layer, and I am also grateful to engineer Maria João de Oliveira for the Raman measurements.

To my father and to my mother who have always supported me. Even when I was having a bad day I knew they would be there to cheer me up. To my grandmother Adelaide now in heaven.

Last but not least, I would like to thank my two insane best friends: Mr. Tiago Gonçalves and Mr. Bunny (Diogo Coelho). They knew exactly when I should stop to have a break (thank you so much for that 1 week pause to travel around Edinburgh/Cambridge together). I am thankful to all my friends (Tiago Gonçalves, Diogo Coelho, Catarina Costa and Jaissica Vassantrai) for their invaluably constructive criticism and friendly advice during my work.

Finally, to my hyperactive dog, Mr. Surf Matias.

Abstract

In this work, zinc oxide (ZnO) and titanium dioxide (TiO_2) nanostructures were grown on different cellulose paper substrates, namely Whatman, office, and commercial hospital papers, using a hydrothermal method assisted by microwave irradiation. Pure ZnO and TiO_2 nanostructures were synthesized, however the growth of TiO_2 above the ZnO was also investigated to produce a uniform heterostructure. Continuous ZnO nanorod arrays were grown on Whatman and hospital papers, however on office paper, it could be observed the formation of nanoplates originating nanoflower structures. TiO_2 nanoparticles homogeneously covered all the substrates and, in some conditions, forming uniform TiO_2 films. The structural characterization was carried out by SEM coupled with EDS, XRD and Raman spectroscopy. The optical characterization of all the materials was carried out. The produced materials were investigated for multifunctional applications, like photocatalyst agents, bacterial inactivators and ultraviolet (UV) sensors. To evaluate the photocatalytic activity under UV and solar radiations, rhodamine B was the model-test contaminant indicator and the best photocatalytic activity was achieved with Whatman paper. Hospital paper with TiO_2 nanoparticles showed significant antibacterial properties against *Staphylococcus aureus*. ZnO-based UV sensors on Whatman demonstrated a responsivity of 0.61 $\mu A\ W^{-1}$.

Keywords: cellulose paper; TiO_2; ZnO; UV sensors; photocatalysis; antibacterial activity.

Resumo

Neste trabalho nanoestruturas de óxido de zinco (ZnO) e de dióxido de titânio (TiO_2) foram crescidas em diferentes tipos de substrato, tais como em papel Whatman, de fotocópia e hospital através de um método hidrotermal assistido por radiação micro-ondas. Produziram-se nanoestruturas de ZnO e de TiO_2 puras, no entanto ainda foi investigada a síntese de TiO_2 por cima do ZnO de forma a produzir uma heteroestrutura uniforme. *Arrays* de nanorods de ZnO contínuos foram crescidos em papel Whatman e de hospital, embora no papel de fotocópia tenha sido possível observar a formação de nanopratos que deram origem a estruturas em nanoflor. As nanopartículas de TiO_2 cobriram de forma homogénea todos os substratos e em algumas condições formaram-se filmes de TiO_2 uniformes. A caracterização estrutural foi feita com recurso ao SEM acoplado ao EDS, XRD e espectroscopia de Raman. A caracterização ótica de todos os materiais também foi realizada. Os materiais produzidos foram testados como agentes fotocatalíticos, inativadores de bactérias e como sensores ultravioleta (UV). Para avaliar a atividade fotocatalítica sob radiação solar e UV, a rodamina B foi usada como poluente modelo e a melhor atividade fotocatalítica foi obtida com o papel Whatman. Papel de hospital com as nanopartículas de TiO_2 apresentou propriedades antibacterianas significativas contra a estirpe *Staphylococcus aureus*. Sensores UV de ZnO em Whatman demonstraram uma responsividade de 0.61 $\mu A\ W^{-1}$.

Palavras-chave: papel de celulose, TiO_2; ZnO; sensores UV; fotocatálise; atividade antibacteriana.

Contents

List of figures

List of tables

Symbols

α – Linear absorption coefficient of the material

θ – Angle

λ – Wavelength

ν – Frequency

A – Value of the antibacterial activity

B – Proportionality constant

C_0 – Average number of CFU on control samples, immediately after inoculation

C_T – Average number of CFU on control samples after 18 h incubation

E_g – Band gap energy

h – Plank's constant

I_{dark} – UV sensor dark current

I_{ph} – UV sensor photocurrent

M – Molar concentration

m – Constant exponent

P_{UV} – Power of the UV source

T_0 – Average number of CFU on nanoparticle impregnated samples, immediately after inoculation

T_T – Average number of CFU on nanoparticle impregnated samples after 18 h incubation

Acronyms

CFU – Colony forming units

EDS – Energy-dispersive X-ray spectroscopy

NRs – Nanorods

RF – Radio-frequency

RhB – Rhodamine B

ROS – Reactive oxygen species

RT – Room temperature

SEM – Scanning electron microscopy

UV – Ultraviolet

VIS – Visible

XRD – X-ray diffraction

Objectives

In this thesis work, ZnO and TiO_2 nanostructures were synthesized through a fast hydrothermal method under microwave irradiation at a low temperature (80 °C), on low-cost cellulose based substrates. The main aims of this work were:

- The preparation of both nanostructures (ZnO nanorods and TiO_2 nanostructures) on several types of paper, including Whatman, office and hospital papers;
- The synthesis of the heterostructure ZnO nanorods/TiO_2 nanostructures. No acid and the use of oxalic acid was investigated for the preparation of TiO_2 nanoparticles, with the aim of preventing the occurrence of chemical etching to ZnO.
- To demonstrate that ZnO, TiO_2 and ZnO/TiO_2 nanostructures can be employed in multifunctional applications, such as photocatalysis, UV sensing and antibacterial activity.

Motivation

ZnO and TiO_2 are metal oxide semiconductors that present several advantages: they are environmentally friendly, abundant, stable, low cost, non-toxic and compatible with wet-chemical routes [1–4]. Microwave irradiation is an appealing method to produce metal oxide nanostructures, since it is fast and offers the possibility of using low temperatures [5,6]. Regarding this method, ZnO and TiO_2 nanostructures can be easily produced and, in addition, be functionalized on cellulose-based substrates [7–9]. To the best of the author's knowledge, ZnO and TiO_2 nanostructures, as well as ZnO/TiO_2 heterostructures grown on various kinds of paper substrates to produce functionalized papers have never been reported before. It is also worth to emphasize the novelty of synthesizing TiO_2 nanostructures using oxalic acid and the differences on ZnO structures regarding the use of each paper-based substrate. By taking advantage from the appealing properties of the 3 nanoplatforms (ZnO, TiO_2, and ZnO/TiO_2) multifunctional materials can be produced.

A growing public health problem, harmful for humans and animals, deals with the contaminated waters. One of the most promising oxidative methods is photocatalysis: this inexpensive method [10] allows the degradation of pollutants from the environment with a low power consumption, and also the degradation of the pollutant can be easily monitored via optical absorption spectroscopy [1,11–14]. RhB has been chosen as the model-test contaminant. This dye is largely used in the textile industry, and in addition it is of great importance, since it is not only hazardous, but also difficult to be removed from the effluents [15].

Moreover, these nanoplatforms have potential as UV sensors and could contribute with further improvements for a better ozone and pollution environment monitoring [16].

Another important topic deals with the several strains of bacteria that are becoming more and more resistant to the conventional antibiotics, such as *S. Aureus*. As a consequence, the number of infection diseases tend to increase in the hospital environment. To prevent this, ZnO and TiO_2 nanomaterials on paper have been reported to be an efficient alternative to inactive bacteria [17–19] .

Considering the importance of the 3 issues mentioned before, in the next pages, ZnO, TiO_2 and ZnO/TiO_2 nanostructures on paper are investigated as photocatalysts, UV sensors and as antibacterial agents.

1. Introduction

1.1 ZnO and TiO_2 nanostructures

Zinc oxide is a *n*-type semiconductor with a direct and wide bandgap of 3.37 eV and has a large free exciton energy of around 60 meV (at room temperature) [5]. ZnO is used in a variety of applications, for instance in thin film transistors [20,21], solar cells [22,23], UV/ozone and glucose sensors [5,24,25], photocatalytic agent [24,26,27] and also as an antibacterial and antifungal agent [5,28]. It has three polymorphs: wurtzite, rock-salt and zinc-blende structures, nevertheless at room temperature, the stable phase of ZnO is hexagonal wurtzite [29]. Wurtzite is composed of zinc cations and oxygen anions in a tetrahedral configuration (**Figure 1.1**) [30,31]. The ZnO polar facets possesses different chemical and physical properties from those presented by non-polar facets, where the polar O terminated facet presents a slightly different electronic structure [32].

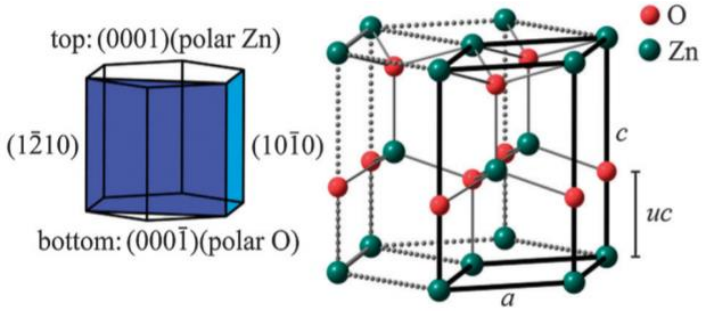

Figure 1.1 – ZnO wurtzite unit cell (*uc*). *a* and *c* are lattice constants [30].

These characteristics are responsible for the vast different properties presented by ZnO, such as piezoelectricity and spontaneous polarization, being a key factor in crystal growth and in defect generation [32]. Indeed, ZnO chemical and physical properties are highly influenced by its size, shape, morphology, crystallinity, as well as the solvents and precursors used to achieve the desired nanostructure [5].

One dimensional ZnO nanostructures, such as nanorods (NRs) have been attracted much attention lately [33]. Generally, they tend to grow faster in polar directions, rather than non-polar facets, which mainly constitute the surface area of the nanorods [30]. They are particularly attractive in the field of sensors, because of their high sensitivity and surface-to-volume ratio. Apart from sensors, this property results in higher density of active sites for surface reactions, which improves the photocatalytic activity. In order to grow ZnO NRs, the deposition of a seed layer is required, in spite of the extra cost [34].

Titanium dioxide is also a *n*-type semiconductor like ZnO and the applications for this material range from sensors to solar cells [7,35–38]. Presently, this material is largely used as photocatalyst [1,2,6,39,40]. From the different phases it might take, the most common ones are

amorphous or the three crystalline phases (represented in **Figure 1.2**): rutile, anatase and brookite [2].

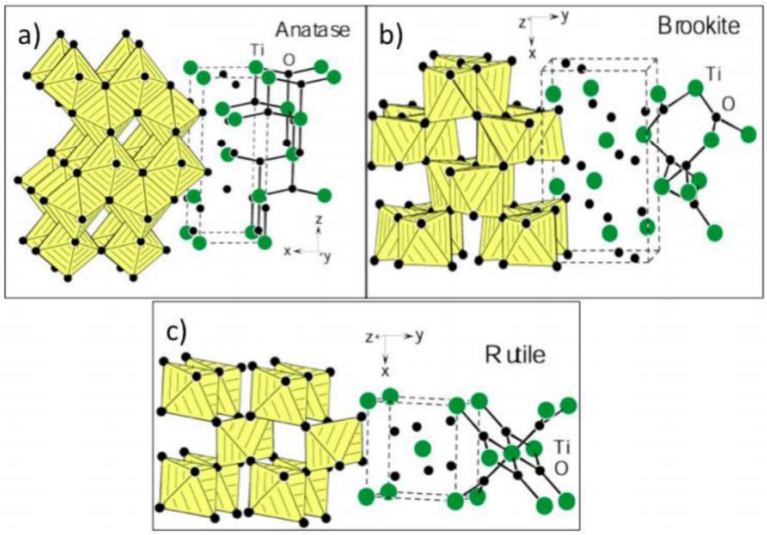

Figure 1.2 – The three crystallographic phases of TiO_2: a) anatase, b) brookite and c) rutile [41].

Anatase has a bipyramid tetragonal symmetry and its structure forms an elongated octahedra, in each four edges are shared (**Figure 1.2**) [41–43]. Rutile is also tetragonal and has 2 formula units for each elementary cell. In the octahedra, two opposite edges are shared forming a linear chain (**Figure 1.2**) [41]. It is the most stable phase whereas anatase and brookite are metastable and with the increase of temperature above 600 ºC they irreversibly and exothermically convert to rutile [44,45]. Brookite has an orthorhombic symmetry with 8 formula units in the elementary cell. Each octahedra has one Ti atom at the center and O atoms at the corners (**Figure 1.2**). Pure brookite is also difficult to synthesize, since it can be easily transformed into the other two forms [41,46]. Therefore, the application of brookite is limited [47].

Anatase is largely used as photocatalyst and it composes the commercial Degussa P25 catalyst. Anatase is considered a better photocatalyst than rutile and brookite. Nevertheless, the photocatalytic behavior of these TiO_2 polymorphs has been under intense debate over the years. For instance, there are several possible reasons generally accepted for anatase to have a better photocatalytic performance than rutile: it possesses higher Fermi level (by 0.1 eV), thus has a lower oxygen affinity, and leads to a higher level of hydroxyl groups on the TiO_2 surface, it has an indirect band gap, while rutile has a direct band gap, resulting in a longer lifetime of photogenerated electron-holes, and also anatase presents a lower average effective mass of photogenerated charges, which increases the rate of electron-holes migration from the bulk to the surface, and as a result the rate of recombination decreases [48–50].

Also, from a recent research, it has been discovered that a mixture of two phases leads to a higher photocatalytic activity in contrast with a purer phase [7,50]. For instance, Boppella *et al.* have reported that the nanocrystals of mixed TiO_2 brookite/anatase and rutile/brookite phases exhibit high RhB degradation under visible light [51]. Nunes *et al.* also showed that films of TiO_2

brookite/rutile phases on cellulose-based substrates have great photocatalytic activity in degrading RhB under solar light [7].

TiO_2 is a wide energy bandgap material, typically displaying optical bandgaps of 3.0 and 3.2 eV for rutile and anatase, respectively [52], and varying from 3.13 to 3.40 eV [46,52,53] for brookite. ZnO as well as TiO_2 are environmentally friendly, earth abundant, chemically stable, low cost, non-toxic and are compatible with wet-chemical synthesis routes [1–4].

1.2 Production of nanostructures on cellulose-based materials

For both materials above described, there are several reports describing the use of hydrothermal/solvothermal synthesis to produce these materials [54–57], while more recently assisted process method by microwave irradiation has been deeply exploited [5,12,19,58]. The main advantages of using the microwave technique to produce nanostructures are its reduced costs, low temperature, short reaction time, high reaction selectivity, low energy consumption and homogeneous volumetric heating [1,5,34]. Another characteristic of the microwave is its high reaction rates [5], due to its ability to instantaneously localize heat into the material [24].

To produce TiO_2, by changing the temperature, synthesis time and pH of the solution, the formation of the amorphous or the tree crystalline TiO_2 phases could be obtained. The type of acid used has also an impact on the crystalline phase composition, morphology and size of the TiO_2 nanoparticles [59].

Among the substrates used, it has been previously reported that cellulose is compatible with wet-chemical synthesis routes [7–9]. Moreover, this material is known as being the most abundant biopolymer on Earth, flexible, inexpensive, among other advantages. All these characteristics make this material highly attractive for nanoelectronics, sensors, photocatalysis and antibacterial applications [7,60,61]. Apart from that, recently the tendency towards the development of multifunctional devices with inexpensive substrates like paper has become the center of several scientific researches [61,62].

1.3 Photocatalysis and UV sensing

Photocatalysis is the acceleration of chemical reactions by photocatalysts which include metal oxides like TiO_2 and ZnO (**Figure 1.3**). When these semiconductors absorb photon energy greater than the bandgap, the electrons from the valence band are excited to the conduction band and an electron-hole pair is created [63]. The electron-hole pair is a strong redox system [48] and in the presence of an absorbed compound in the photocatalyst surface has the ability to reduce and/or oxidize the compound [48,64,65]. As a result, the electrons will reduce oxygen on semiconductor surfaces, generating superoxide radicals and hydroperoxide radicals (•OHH) upon further reaction with H^+. The holes will oxidize OH^- and water molecules at the surface producing hydroxyl radicals (•OH) [19,48,63]. These superoxide ions, hydroxyl radicals and hydroperoxide radicals

(ROS: reactive oxygen species) will after interact with the dye and originate a range of intermediates to finally decompose the organic/inorganic compounds [12,65].

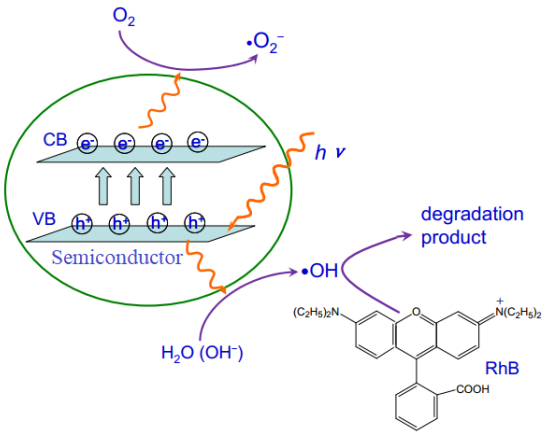

Figure 1.3 – Photocatalytic mechanism of RhB degradation with a semiconductor (such as TiO_2 or ZnO) (adapted from [66]).

The mechanism observed for UV sensing is similar to photocatalysis. The semiconductor photoconductivity relies on the electrical conductivity changes under irradiation. The photodetection is also governed by a hole-trapping mechanism based on the adsorption/desorption of chemisorbed oxygen molecules at the surface [67].

Since TiO_2 and ZnO have similar band gap energies, the photocatalytic activity should not differ much. However, for ZnO in aqueous solution, there is a decrease of photocatalytic activity due to photocorrosion that normally occurs under UV light illumination [19].

Two main limitations of these semiconductors (ZnO and TiO_2) are the wide band gaps. As a consequence, they mainly absorb in the UV part of the spectrum and have low quantum yield as photocatalysts [68]. However, the percentage of UV light that reaches earth is relatively small (3-5 %) and so their efficiency and application is limited. As a result, it is imperative to extend their absorption range to the visible region [7,69]. One alternative to enhance the absorption of visible light is through the modification of the catalyst's morphology which affects the separation of charges and consequently the available active sites. Other possibilities include annealing to improve crystallinity, the use of a capping agent to inhibit the growth in some directions and expose the more reactive facets, defect manipulation, doping and the use of composites/heterostructures [58,70]. A promising strategy is the production of an heterostructure, such as ZnO/TiO_2. An improvement in charge separation and therefore a reduction in recombination is expected. TiO_2 has similar physico-chemical properties to ZnO and TiO_2 in anatase phase (3.2 eV) presents a smaller and closer band-gap to ZnO (3.37 eV) [71]. Hence, the use of these heterostructures have potential in photocatalytic and UV sensing applications [68,72,73].

1.4 Antibacterial activity

Metal oxide (such as ZnO and TiO_2) nanostructures have a lot of potential as antimicrobial agents, against both gram-positive and gram-negative bacteria, because of their capability and high selectivity, for instance in biological and pharmaceutical applications [74–76].

On one hand, when ZnO and TiO_2 nanoparticles are photoactivated, ROS products are generated and upon contact with bacteria, they promote the damage of the cell wall, with a subsequent peroxidation of the polyunsaturated phospholipids of the lipid membrane. On the other hand, if nanoparticles are small, they can penetrate the cell triggering these processes internally. It has been reported that this photocatalytic disinfection is determined by the rigidity and chemical arrangements on the surface cell structure. Also, the high surface area-to-volume ratio and the physicochemical properties of the nanomaterials can highly influence the inactivation mechanism of bacteria [77]. However, a lot of uncertainties still remain related to the type of bacteria that are more sensitive to ZnO and TiO_2 nanoparticles [17,19,74,76].

The two semiconductors are efficient antimicrobial agents that when combined can increase the absorbance solar spectrum energy of TiO_2 up to 15%, hence enhancing TiO_2 photocatalytic activity, which improves the generation of ROS that will at last inhibit the capability of microorganisms [19,74,76].

The bacteria strain that has been chosen for this study was *S. Aureus*, since it is responsible for causing several infections on health individuals or patients with problems in the immune system, it has the ability to colonize the skin and nares and of being transmitted in hospital centers. Furthermore, this gram-positive bacteria is well known for being resistant to the most commonly used antibiotics, such as penicillin and oxacillin [78].

Bacteria can be separated in two groups: the gram-negative and gram-positive. Gram-negative microorganisms have a thin peptidoglycan cell wall surrounded by an outer membrane of lipopolysaccharide which works as a permeable barrier against toxic molecules from the outside. Gram-positive microorganisms only have a thick wall of peptidoglycan, without any other membrane [79,80].

Studies had shown that *S. Aureus* is extremely susceptible to ROS products with a well-defined zone of inhibition (when performing the Kirby-Bauer Test) upon contact with high concentrations of TiO_2 [28,80,81]. In the present thesis, a new study is proposed: the antibacterial assay by the absorption method, in order to investigate the efficiency of *S. Aureus* inactivation by TiO_2 nanostructures on paper.

2. Experimental Procedure

2.1 ZnO and TiO_2 synthesis

The ZnO and TiO_2 nanostructures have been produced using a hydrothermal synthesis assisted by microwave irradiation. Three different types of papers have been used, *i.e.* Whatman grade 2, office paper from INAPA Tecno Super Speed and commercial hospital paper coming in a coach roll. For the ZnO nanostructures, a seed layer had to be previously deposited on paper substrates [9,34], while for TiO_2 no previous treatment on paper surface has been carried out [7]. The RF sputtering conditions were previously reported in ref. [9], however with a power of 50 W (further details in **Appendix B1**). Prior to microwave synthesis, the ZnO seed layer had a subsequent UV treatment (Novascan PSD UV-Ozone system) of 5 min [9] to remove surface contaminants and to obtain a more polar surface of the ZnO seed layer that will improve the growth of ZnO nanostructures. The ZnO aqueous solution was composed by 25 mM zinc nitrate hexahydrate ($Zn(NO_3)_2 \cdot 6H_2O$; 98%, CAS: 10196-18-6) and 25 mM hexamethylenetetramine ($(C_6H_{12}N_4)_2$; 99%, CAS: 100-97-0) both from Acros Organics [9]. For TiO_2 nanostructures, the titanium (IV) isopropoxide ($Ti[OCH(CH_3)_2]_4$) used was from Sigma-Aldrich (97 %), CAS: 546-68-9. In a typical synthesis, 50 mL of deionized water is mixed with 10 mL of oxalic acid dihydrate ($C_2H_2O_4 \cdot 2H_2O$, CAS 6153-56-6, Merck Millipore). The molar concentration of acid was fixed 1 M, nevertheless to produce the heterostructure, the molar concentration of 25 mM was also tested. Moreover, also in the case of the ZnO/TiO_2 heterostructure, the synthesis with no acid was investigated (60 mL H_2O). In the case of ZnO, the seed layer was facing down [1,2,34]. Temperature, power and maximum pressure of the microwave (CEM Focused Microwave Synthesis System Discover SP) were kept respectively at 80 °C and 100 W for all materials. The microwave pressure was set to 150 Psi for TiO_2 and 300 Psi for ZnO nanostructures. The synthesis time was 15 min for ZnO and 15 min or 30 min for TiO_2 depending on the application selected. For the heterostructure, ZnO and TiO_2 microwave synthesis time was maintained at 15 min. After each synthesis, the paper substrates were cleaned with deionized water and left drying overnight at room temperature.

2.2 Photocatalytic activity

The photocatalytic activities of the ZnO and TiO_2 nanostructures, as well as the ZnO/TiO_2 heterostructure was evaluated at room temperature (RT) considering the degradation of RhB from Sigma Aldrich under a solar light simulating source and UV radiation. All the experiments were performed according to the International standard ISO 10678 [1]. The experimental details are described in **Appendix B2**. For the solar light exposure, it was used a LED solar simulator LSH 7320 (AM 1.5 spectrum) with an intensity of 100 mW/cm^2. For the UV exposure, a mercury lamp

model HNSL from Osram Puritec was used with a power of 95 W. Absorption spectra were recorded using a PerkinElmer lambda 950 UV/VIS/NIR spectrophotometer with different time intervals up to a total of 21 h for solar radiation and 15 h for UV exposure.

2.3 UV sensing

The synthesized ZnO nanostructures were characterized as a UV sensor on paper substrates with a potentiostat model 600, from Gamry Instruments, in a chronoamperiometry configuration, applying a continue +10 V voltage. For interdigital electrical contacts, a carbon ink was screen-printed (mesh 120T). The produced materials were subjected to irradiation with an ultraviolet lamp, UVM-28 EL Series UV Lamp, 8 W at a wavelength of 302 nm. The experiments were performed with UV light irradiation for 3 min followed by 3 min in off state during 4 cycles [5].

2.4 Quantitative assay for antibacterial study: absorption method

The antibacterial activity of hospital paper samples with TiO_2 synthesized for 15 min (1 M) was evaluated against *Staphylococcus aureus* ATCC6538 by the absorption method according to ISO 20743:2013(E), 2013 standards, Textiles – Determination of Antibacterial Activity of Textile Products, Second Edition, 2013) [79]. The paper samples were cut with a CO_2 laser (Universal Laser Systems VLS 3.5) in circles (3.5 cm diameter) with TiO_2 or without (control) and exposed to UV radiation for 30 min on both sides. Then, bacterial suspension was directly inoculated into samples. The antibacterial activity was evaluated quantitatively by comparing the number of CFU (Colony Forming Units) on the surface of paper with TiO_2 nanoparticles and control paper after incubating at 37 ºC for 18 h [28].

2.5 Characterization techniques

Surface SEM observations were carried out using a Carl Zeiss AURIGA CrossBeam FIB-SEM workstation and equipped for EDS measurements. The dimensions of the nanostructures have been determined from SEM micrographs using the ImageJ [82] software and considering 30 distinct structures for each measurement.

XRD and Raman spectroscopy measurements were carried out for the ZnO and TiO_2 nanostructures, but also for the heterostructure. Micro-Raman spectroscopy experiments were carried out with in Via Qontor Confocal Raman Microscope from Renishaw, equipped with a 150 mW He–Ne laser operating at 532 nm. XRD measurements were carried out in a X'Pert PRO PANalytical powder (X'Pert diffractomer using Cu Kα line radiation (λ = 1.540598 Å)). Diffraction patterns were recorded from 20° to 70° (detector angle 2θ) with a step of 0.0330º in a Bragg-Brentano configuration. The simulated brookite corresponds to ICDD file No. 01-076-1937, simulated rutile to ICSD file No. 96-900-4143 and the simulated anatase to ICSD:

082084 with a (Å)= b (Å)= 3.7830 and c (Å) = 9.4970. The simulated zinc oxide corresponds to ICSD file No. 00-036-145.

Room temperature diffuse reflectance measurements were performed according to [9] with a PerkinElmer lambda 950 UV/VIS/NIR spectrophotometer (details in **Appendix B3**).

3. Results and discussion

ZnO and TiO_2 nanostructures, as well as ZnO/TiO_2 heterostructures were successfully synthesized under microwave irradiation using cellulose-based substrates at low temperatures and fast synthesis times. The distinct substrates were selected due to their specific application targets. Whatman is a chromatography paper, being composed by highly pure cellulose, without any additives. This paper was thought for photocatalysis and UV sensing applications. Office was also selected for photocatalysis, but in terms of high abundancy and low cost to obtain a disposable photocatalytic paper. At last, hospital paper was selected for the antibacterial activity experiments in a way to avoid growth and proliferation of microorganisms commonly found in the hospital environment, and besides it is a disposable paper. This latter paper was also tested for photocatalysis. The produced nanostructures, as well as the ZnO/TiO_2 heterostructure, substrates and final devices were systematically investigated, and multifunctional materials were produced.

3.1 Morphological and structural characterization

3.1.1 SEM/EDS analysis

Figure 3.1 shows the ZnO nanostructures synthesized under microwave irradiation and using Whatman (a), office (b) and hospital (c) papers as substrates. Microwave irradiation resulted in uniformly covered substrates forming continuous ZnO nanostructured arrays with two distinct film characteristics. Whatman and hospital papers resulted in continuous ZnO nanorod arrays, while on office paper it has been observed nanoplates originating flower-like structures. An analogous study had previously demonstrated the growth of ZnO nanorod arrays on Whatman paper [9].

The discrepancies observed on these three types of papers are thought to be related to the impurities present on the substrates, *i.e.* calcium carbonate ($CaCO_3$). EDS analyses were carried out on the pristine paper substrates and the results are presented in **Figure A.1**. Both office and hospital papers revealed the presence of Ca appearing as agglomerates. Some minimal traces of Al and Si were also observed on hospital paper. Whatman paper, on the other hand, is highly pure, presenting just C and O.

Some studies performed demonstrated the effect of adding calcium carbonate and ZnO, as well as the interaction between these materials [83,84]. In Ref. [85], it has been demonstrated that $CaCO_3$ effectively changes the physical properties of ZnO. Moreover, Tian *et al.* [86] demonstrated that the ZnO synthesis with sodium citrate originate plates instead of nanorods, in a way that citrate ions strongly bind to the Zn atoms on the (002) surfaces resulting in hexagonal ZnO nanoplates. A similar effect is expected to have occurred with ZnO and the calcium carbonate present on office paper, in which the ZnO-rod like structure growth along the ⟨001⟩

orientation was hindered, producing plates. Comparing both office and hospital papers, where calcium carbonate was detected (**Figure A.1**), it has been observed the presence of this element in higher amounts in office paper [87]. In the case of Whatman paper, the ZnO average nanorod lengths were 160.7 ± 3.4 nm, while in the case of hospital paper, the values were 128.6 ± 4.3 nm. The length of the plates' structures observed on office paper could not be certainly determined.

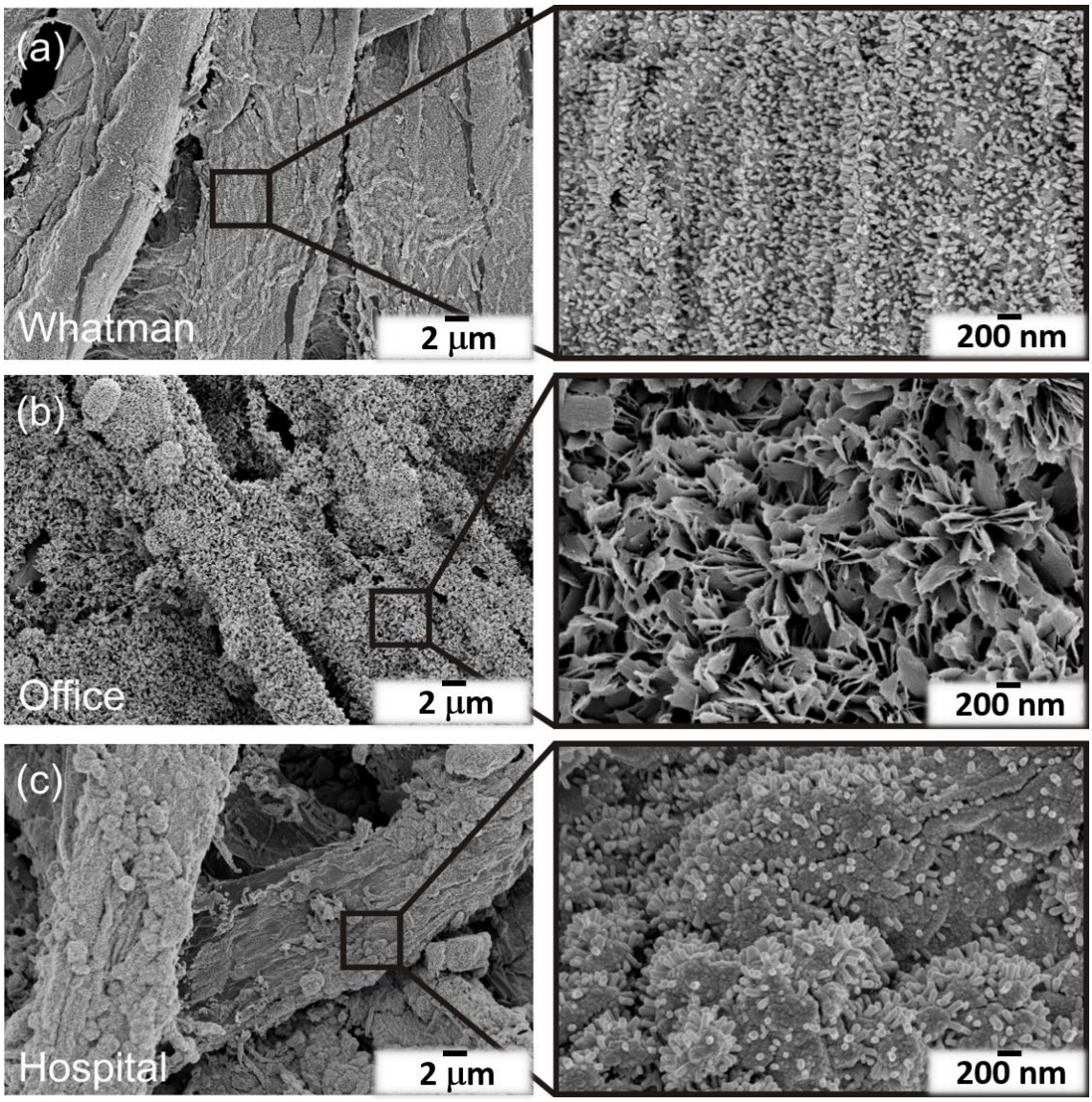

Figure 3.1 – ZnO nanostructures grown on (a) Whatman, (b) office and (c) hospital papers. The insets magnify the nanostructures synthesized.

Figure 3.2 depicts the TiO_2 nanoparticles and films synthesized under microwave irradiation and using Whatman (a), office (b) and hospital (c) papers as substrates. In the case of hospital substrate two synthesis times were investigated, that is 15 and 30 min. As observed for ZnO materials, the microwave irradiation also resulted in uniformly covered substrates, without any seed layer. Individual nanostructured particles with an undefined structure mostly covered the surface, and in some cases forming larger agglomerates. In some conditions, the nanoparticles grew forming films on the substrate surfaces. The film synthesized on Whatman paper was composed

by dense agglomerates of TiO_2 nanoparticles, while a thinner film could be seen on the office paper. On hospital paper, these individual nanoparticles were randomly distributed, and in some cases appearing as agglomerates, but in smaller amounts when compared to the ones observed on Whatman paper. The average diameter of the nanoparticles synthesized on Whatman paper was 147.6 ± 26.6 nm. In the case of the nanoparticles formed on hospital paper with 15 min of microwave synthesis, the average size was determined to be 29.5 ± 1.9 nm, while in the case of 30 min synthesis, the average size was 30.5 ± 5.5 nm (see **Table 3.1**). The nanoparticles formed on the office paper substrate could not be easily distinguished and have not been measured.

Comparing both conditions investigated on hospital paper it has been observed that with a 30 min synthesis, slightly larger nanoparticles were formed (in average), and the agglomerates became greater in size (not so many isolated nanoparticles were detected). And for that reason, the 15 min synthesis condition was selected for the antibacterial activity experiments, while the 30 min, was used for photocatalysis. Moreover, smaller nanoparticles could more easily penetrate the permeable membrane of bacteria [79]. The heterogeneities and roughness of the cellulose fibers did not allow the determination of thicknesses from the materials produced.

EDS analyses were carried out in both ZnO and TiO_2 materials confirming the well distributed materials along the substrates (**Figure A.2**). As previously observed in an analogous study, all the TiO_2 films were grown on both sides of the cellulose-based substrates [7].

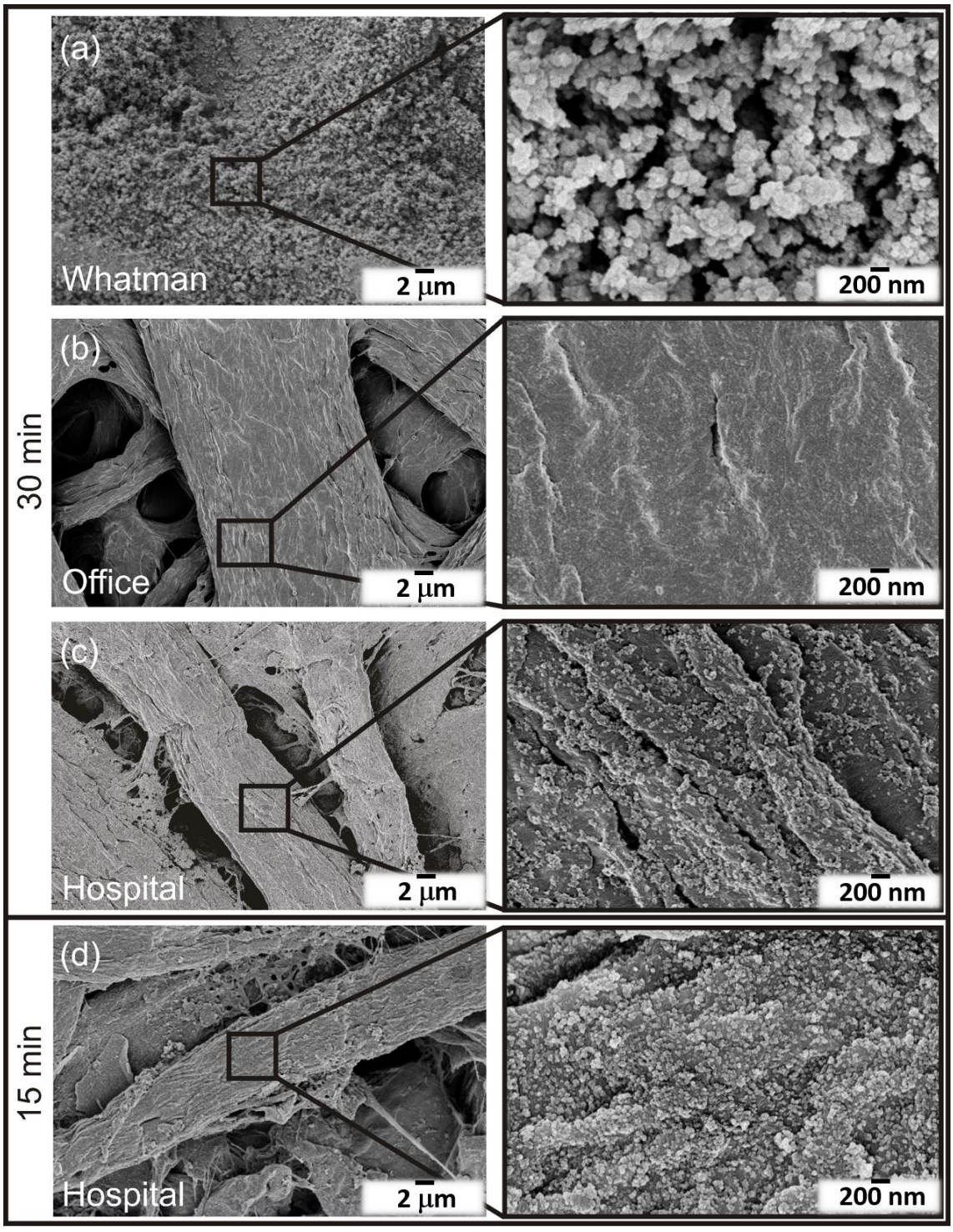

Figure 3.2 – TiO_2 nanostructures grown on (a) Whatman, (b) office and (c) hospital papers at 30 min synthesis time. (d) TiO_2 nanostructures synthesized at 15 min. The insets magnify the nanostructures formed after microwave synthesis.

The ZnO/TiO_2 heterostructures were also successfully produced under microwave irradiation using paper-based substrates. Nevertheless, the ZnO/TiO_2 heterostructure on hospital paper-based materials have not been investigated, since the paper is easily folded after synthesis, making it difficult to work with, especially after two individual microwave syntheses. To prevent the chemical attack of ZnO, the oxalic acid concentration was expressively decreased (1 M to 25

mM), and also the TiO_2 synthesis was performed without any acid. **Figure 3.3** shows the ZnO/TiO_2 heterostructures grown on Whatman and office papers with (25 mM) or without oxalic acid. The effect of acid-based TiO_2 syntheses was evident on ZnO nanostructures present on both substrates. In **Figure 3.3 (b)** it is clear the etching of the ZnO nanorods after 15 min TiO_2 microwave synthesis. The average ZnO nanorod length decreased to 95.6 ± 2.0 nm in Whatman paper (**Table 3.1**). The ZnO acid chemical etching has been reported previously [88,89]. Nevertheless, oxalic acid was expected to have low impact on ZnO nanostructure, since it has been reported the use of oxalic acid to synthesize ZnO [90,91]. On office paper, the etching effect was also observed with deterioration of the plate surface and appearance of laminar structures together with occurrence of holes (see inset on **Figure 3.3 (d)**). Regarding the presence of TiO_2, the individual nanoparticles grew surrounding the ZnO nanorods on Whatman paper, as can be seen on the **Figure 3.3 (a)** inset. The presence of TiO_2 agglomerates was also detected in some conditions. Nevertheless, uniformly TiO_2 films covered all the substrates as previously observed in **Figure 3.2**, and as attested by EDS analyses (**Figure A.2**). In the case of office paper, the individual nanoparticles were not discernible, however a thin film is believed to have covered the ZnO nanostructures, such as presented in **Figure 3.2 (b).**

Table 3.1 – Summary of ZnO nanorod lengths (averages) for pure ZnO, ZnO/TiO_2 heterostructure and TiO_2 nanostructure diameters (averages) using different types of paper and synthesis times.

	Pure ZnO nanorod lengths		ZnO nanorod length (in the heterostructure)		TiO_2 nanostructure diameters	
Type of paper	Average number (nm)	Average standard deviation (nm)	Average number (nm)	Average standard deviation (nm)	Average number (nm)	Average standard deviation (nm)
Whatman	160.7	3.4	95.6	2.0	147.6	26.6
Hospital (15 min)	128.6	4.3	-	-	29.5	1.9
Hospital (30 min)	-	-	-	-	30.5	5.5

The EDS analyses of the ZnO/TiO_2 heterostructure formed on Whatman paper is presented in **Figure A.2 (m)**, and it could be observed the homogeneous distribution of Zn along the substrate (**Figure A.2 (p)**), and Ti in a lower extend. TiO_2 agglomerates were clearly identified in **Figure A.2 (q)**, and this may be a possible reason for the lower concentration of Ti detected in just a small region of the sample (**Figure A.2 (m)**), when compared to **Figure A.2 (e)**. Another plausible explanation for the low Ti detected could be the lower molar concentration used for the heterostructure resulting in lower TiO_2 nanoparticles' formation along the substrate.

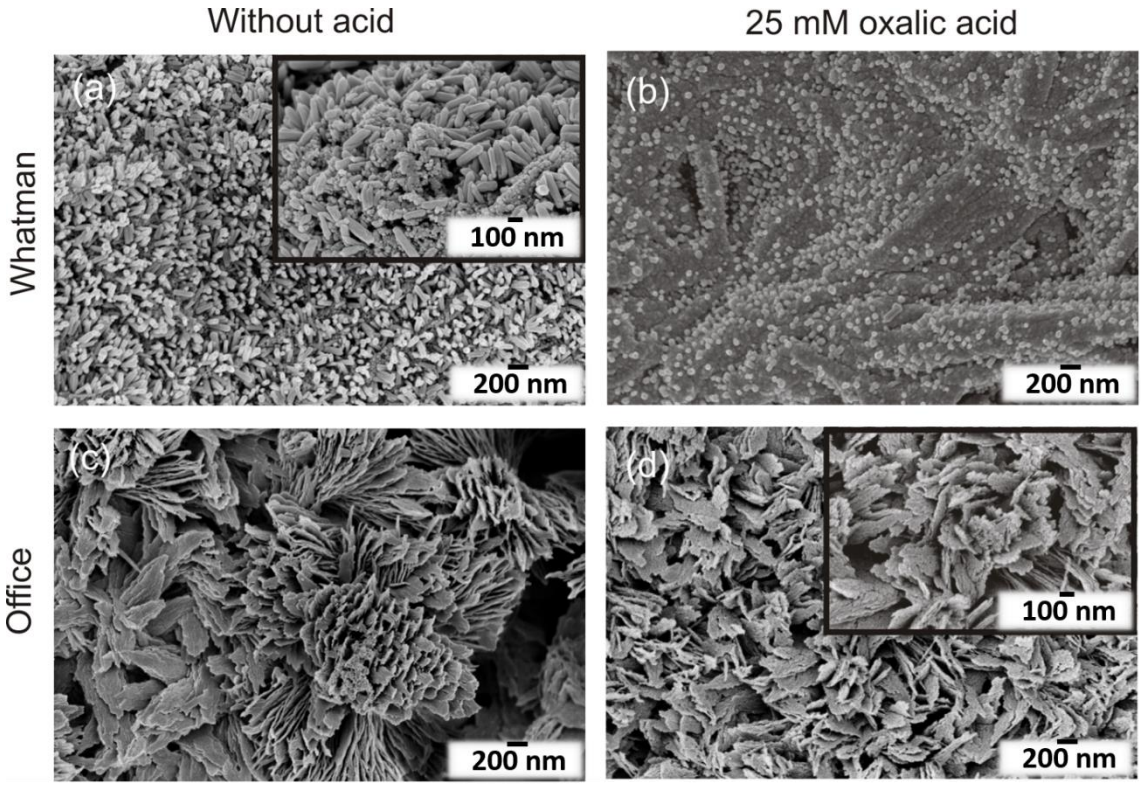

Figure 3.3 – ZnO/TiO_2 heterostructures grown on Whatman paper having TiO_2 synthesized (a) without acid and (b) with 25 mM of oxalic acid; and office paper (c) without acid and (d) with 25 mM of oxalic acid. The ZnO and TiO_2 nanostructures were both synthesized considering 15 min of synthesis time. The insets in (a) magnifies the heterostructure, while on (d) evidences the surface modification with oxalic acid.

3.1.2 XRD and Raman spectroscopy measurements

The materials grown on Whatman paper were the only measurements presented, since office and hospital papers displayed XRD peaks [87] and intense fluorescence on Raman measurements coming from the calcium carbonate [92,93]. Nevertheless, a substantial contribution from the Whatman substrate was also observed on both techniques, hindering the ZnO or TiO_2 signals (**Figure A.3**). Moreover, the greater contribution coming from the substrates is also associated to the reduced thickness of the metal oxide-based films/arrays produced, especially in the case of TiO_2. The XRD results (**Figure 3.4 (a)**) show that the characteristic peaks of native cellulosic fibers: $(1\bar{1}0)$, (110), (200) and (004) at $2\theta = 14.9$ °, $2\theta = 16.6$ °, $2\theta = 22.7$ ° and $2\theta = 35$ °, are respectively in agreement with the literature [9]. No impurities or other crystallographic phases were detected. In **Figure 3.4 (a)**, it could be confirmed the growth of ZnO nanostructures on cellulosic based substrates. The observed hexagonal wurtzite ZnO peaks were identified as the crystallographic planes (100), (002), (101) and (110). An analogous study also demonstrated the formation of pure ZnO on Whatman paper grown under microwave irradiation [9]. In the case of TiO_2, the paper signal totally obscured its signal. The XRD measurements of the ZnO/TiO_2 heterostructure were also inconclusive, since TiO_2 could not be identified and the reduced size of ZnO due to chemical etching may have contributed to the lack of ZnO signal coming from the material. As an alternative for TiO_2 phase identification, it has been analyzed

the powder formed during the microwave synthesis. ZnO in the form of powder is also presented for comparison (**Figure 3.4 (b)**). XRD results confirmed that the produced material is fully assigned to the hexagonal wurtzite ZnO crystalline structure. In the case of TiO_2, all peaks in the experimental diffractograms could be assigned to the anatase phase. No peaks associated to impurities such as $Ti(OH)_4$ were detected and all the peaks suggest that the materials are well crystallized. Several studies reported the formation of anatase TiO_2 under microwave irradiation [94–96], nevertheless to the best of author's knowledge, the production of anatase TiO_2 nanostructures grown on paper substrates under microwave irradiation has never been reported before.

The effect of oxalic acid on TiO_2 crystal growth has been reported by Fahmi *et al.*[97]. It has been stated that the growth of rutile is favored, because oxalic acid binds more strongly to anatase. Moreover, it has been suggested that oxalic acid undergoes dissociation (splitting of both H atoms), and the resulting oxalate ion, $C_2O_4^{2-}$ is bonded through the oxygen atom to neighboring Ti atoms [42]. In the present study, all the microwave syntheses led to the formation of pure TiO_2 anatase instead of rutile. This behavior may be resultant of microwave synthesis and its characteristics, such as microwave coupling efficiency to the solvent, heating rate, among others.

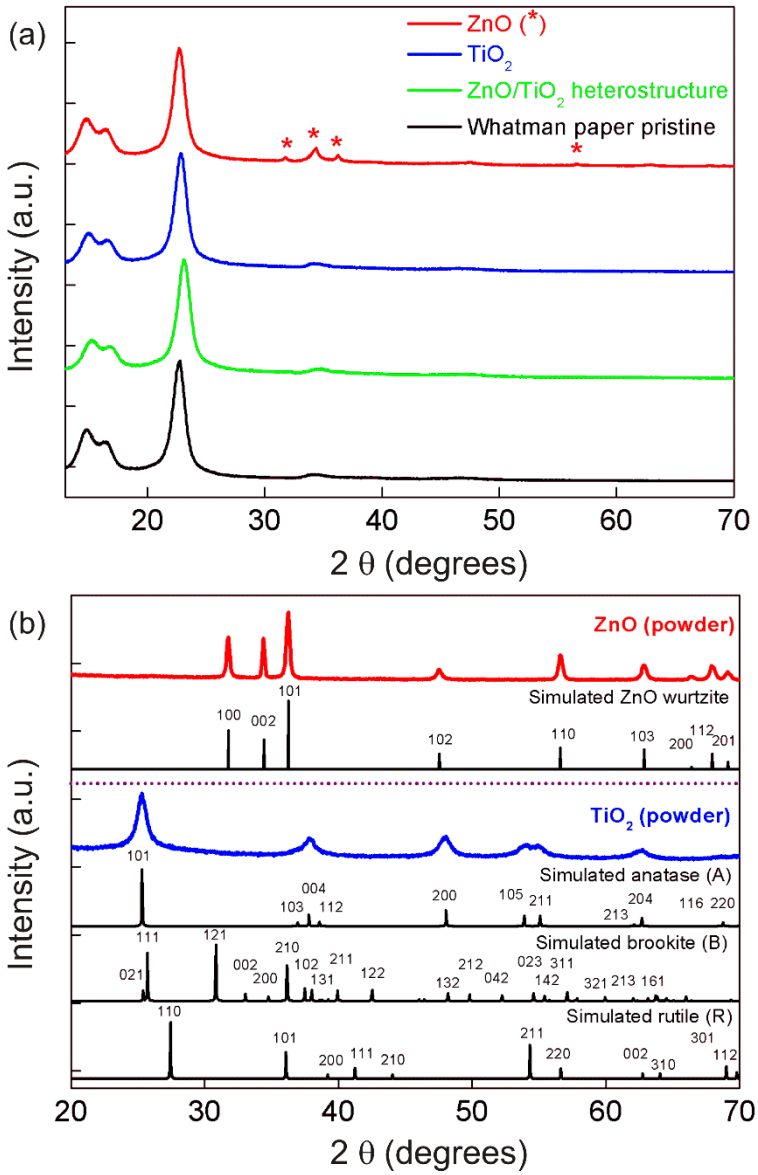

Figure 3.4 – (a) XRD diffractograms of ZnO and TiO_2 (1 M, 30 min) nanostructures grown on Whatman paper substrate. The ZnO/TiO_2 (25 mM) heterostructure-based material is also presented together with the Whatman pristine paper. The ZnO peaks are identified with asterisks (*). (b) ZnO and TiO_2 powder produced during microwave synthesis. The simulated ZnO wurtzite, TiO_2 anatase, rutile and brookite structures are presented.

3.2 Optical characterization

The optical bandgap values for TiO_2 and ZnO nanostructures together with the ZnO/TiO_2 heterostructure were presented in **Figure 3.5**. Reflectance data was acquired to evaluate the optical bandgap through Tauc plot. Based on equation 3.1, it is possible to determine the optical bandgap (E_g) by plotting $(\alpha h\nu)^{\mathrm{m}}$ against $h\nu$ and through the extrapolation of the linear part with 0:

$$(\alpha h\nu)^{\mathrm{m}} = \mathrm{B}(h\nu - E_g) \qquad (3.1)$$

where α is the linear absorption coefficient of the material, $h\nu$ is the photon energy, B is a proportionality constant and m is a constant exponent which determines the type of optical

transitions (m = 2 is for direct allowed transitions and m = 1/2 for indirect transitions) [7,34]. The bandgaps of the nanostructures on hospital and office papers were not presented due to the high influence (high reflectance peaks) coming from the paper substrates. For ZnO nanorods it was considered a direct optical bandgap, while for TiO_2, it has been assumed that the nanostructures are from anatase phase as observed in XRD measurements (**Figure 3.4 (b)**), and for that case with an indirect optical bandgap.

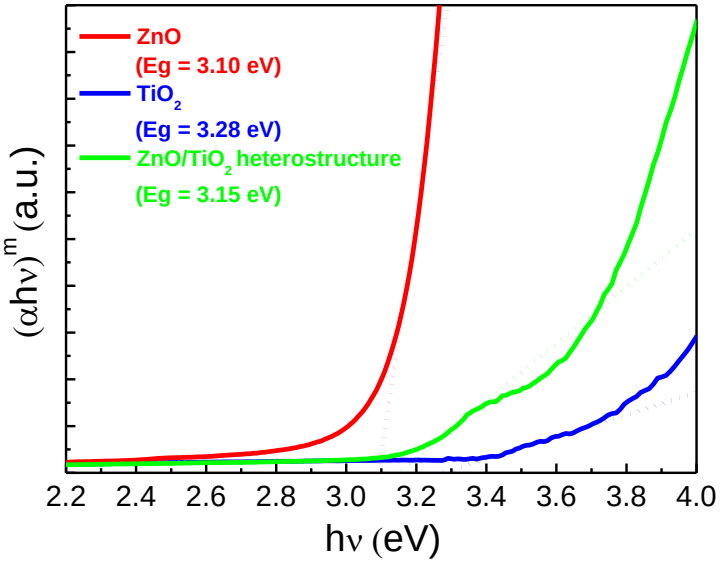

Figure 3.5 – $(\alpha h\nu)^m$ versus photon energy $h\nu$. The optical bandgap measurements were carried out for the ZnO (15 min) and TiO_2 nanostructures (1 M, 30 min), as well as the ZnO/TiO_2 heterostructure (25 mM)*. All materials have been grown on Whatman paper.
***note:** Tauc plot cannot be used to calculate the optical band gap value of the heterostructure, since a mixture of 2 phases is visible. Ellipsometry could be an alternative to evaluate the band gap energy.

The bandgaps estimated were 3.10, 3.28 and 3.15 eV for ZnO and TiO_2 nanostructures and ZnO/TiO_2 heterostructure, respectively. These values are in agreement with the ones reported in the literature, that is between 3.1 and 3.3 eV for ZnO [98,99], and around 3.2 eV for anatase TiO_2 [1,49]. The ZnO bandgap value is in agreement with an analogous study, in which ZnO nanorods were fabricated on Whatman paper [9]. For the ZnO/TiO_2 heterostructure, an intermediate value between both pure materials was obtained, and so the bandgap value is expected to be a contribution of both nanostructures (TiO_2 and ZnO).

3.3 Photocatalytic activity

ZnO and TiO_2 have been largely used in photocatalysis, in which the latter continues to be one of the most widely embraced photocatalysts nowadays [1,2,6,7]. ZnO and TiO_2 are wide bandgap materials, which makes them active under UV light irradiation and thus it is expectable that both materials have higher photocatalytic activity under UV than under solar radiation [1].

Nevertheless, in terms of pollutant degradation with UV irradiation, this procedure is extremely limited, and the use of the complete solar spectrum is highly desired. In the present study, both ZnO and TiO_2 have been exposed to UV and solar radiation, however ZnO and the

ZnO/TiO_2 materials did not show any significant RhB degradation (results not shown) under solar radiation, and for that matter, just TiO_2 materials are presented in **Figure 3.6**.

The photocatalytic activity of TiO_2 grown on Whatman and hospital papers was evaluated through the degradation of rhodamine B under solar radiation, and the results are presented in **Figure 3.6**. The material grown on office paper did not reveal any RhB degradation under solar radiation, and it is expected to be due to the reduced thickness of the film produced (**Figure 3.2 (b)**). The condition analysed for the photocatalytic experiments was 1 M and 30 min, since dense/larger agglomerates of TiO_2 nanoparticles were produced (**Figure 3.2)**. The maximum absorption peak of RhB is in accordance with the literature and in aqueous solution is located at 554 nm [100]. For both Whatman and hospital paper-based TiO_2 materials, it is clearly visible and previously stated in other studies, that the RhB degradation is accompanied by a slight hypsochromic shift of absorption bands [101]. The TiO_2 Whatman-based material (**Figure 3.6 (a)**) achieved a degradation value of 57 % when compared to 50 % of degradation observed in hospital-based material (**Figure 3.6 (b)**), both after 21 h of solar light exposure. Thus, a comparable degradation behavior could be observed for both materials under solar radiation.

It has been proposed that under the exposure of solar light, RhB degradation results in N-deethylation, cleavage of chromophore with the final mineralization of the dye [7,102].

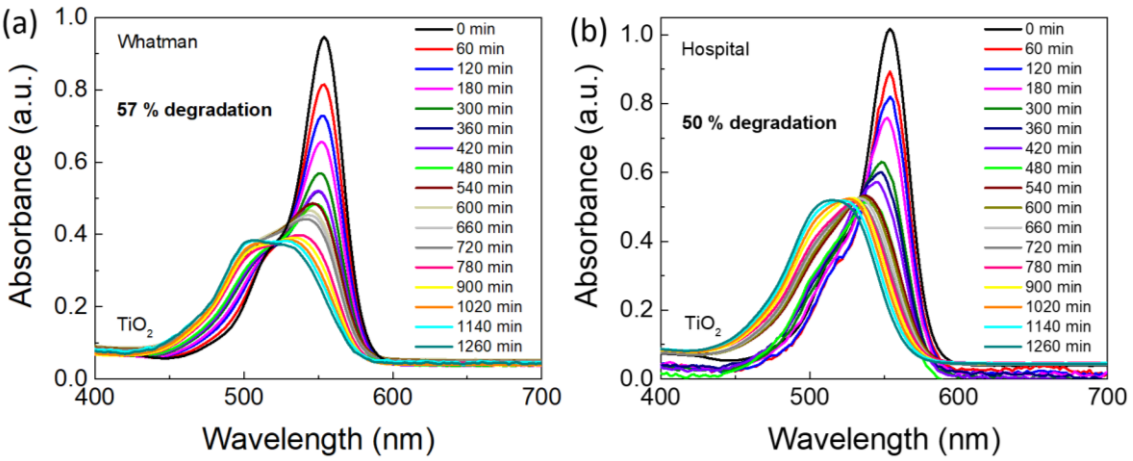

Figure 3.6 – RhB absorbance spectra under simulated solar light radiation (led simulator with AM 1.5 spectrum) up to 21 h for TiO_2 nanostructures grown on (a) Whatman and (b) hospital papers (1 M, 30 min synthesis time) at room temperature.

The photocatalytic activity of ZnO and TiO_2 nanostructures, together with the ZnO/TiO_2 heterostructure was also evaluated through the RhB degradation efficiency under UV irradiation. In the case of ZnO nanostructures, the hospital paper resulted in smaller nanorods, which compromised its photocatalytic performance also under UV irradiation. In the case of TiO_2, as observed in solar radiation experiments, the office paper-based materials did not reveal significant photocatalytic activity under UV irradiation and the results have not been presented. The photocatalytic activity of ZnO nanostructures grown on Whatman and Office papers is presented in **Figure 3.7 (a)** and **(b)**, respectively. A RhB degradation of 40 % and 51 % was obtained in

15 h of UV exposure, for ZnO nanostructures grown on Whatman and office papers, respectively. The highest photocatalytic activity observed on office-based materials is expected to be related to the higher surface/volume ratio of the nanoplates forming the flower-like structure (**Figure 3.1**) which results in higher density of active sites for surface reactions. Moreover, the morphology and the specific crystal facets play an important role in ZnO catalytic properties, since different crystal facets have different dangling bond configurations [24]. No contribution from different phases are expected on ZnO, since all materials are expected to have the hexagonal wurtzite ZnO structure. The optical bandgap could not be determined for most of the paper-based substrates, so no direct conclusion can be stated (**Figure 3.5**).

In the case of TiO_2, as investigated in solar radiation experiments, Whatman and hospital-based materials were also exposed to UV irradiation. Identical RhB degradation values to the solar radiation experiments were obtained under UV irradiation, *i.e.* 57 % for the TiO_2 Whatman-based material and 50 % for the hospital-based one. Nevertheless, significant smaller exposure time was required (15 h instead of 21 h). Nevertheless, the higher photocatalytic under UV than under solar simulating light source is expectable, since TiO_2 is a wide bandgap semiconductor [1,7].

The enhanced photocatalytic activity of TiO_2 is also related to the presence of the anatase phase. Anatase is considered a better photocatalyst than other TiO_2 polymorphs, *i.e.* rutile and brookite, as mentioned in the introduction. One possible reason for anatase better photocatalytic performance is its indirect bandgap that exhibits a longer lifetime of photoexcited electrons and holes when compared to the direct bandgap rutile and brookite [49].

In terms of active facets, the reactivity of the facets also differ, in anatase the active facets are {111}>{001}>{100}>{101} [70], thus some contribution coming from them are expected. Regarding the size effect, the TiO_2 nanoparticles observed on Whatman paper were expressively larger than the ones on hospital paper. Moreover, a better and more dense coverage of the substrate was also observed on Whatman-based substrates with the formation of larger agglomerates (**Figure 3.2**). As a result, more catalyst is available during reaction, which could increase the absorbance of incident light and thus the generation of charge carriers [102].

The photocatalytic activity of ZnO/TiO_2 heterostructures has also been investigated under UV irradiation. Both TiO_2 syntheses with and without acid have been tested. In **Figure 3.7**, it is presented the results of the ZnO/TiO_2 heterostructure having TiO_2 synthesized without acid on Whatman and office papers. The combination of nanostructures was expected to improve the photocatalytic activity, decreasing the recombination of electron-hole pairs and increasing the lifetime of carriers. As a result, there should be an improvement in the interfacial charge transfer and thus in the redox reactions [73]. This, however, was not observed on Whatman (**Figure 3.7 (e)**) and office paper-based materials (**Figure 3.7 (f)**).

In fact, comparing the ZnO Whatman-based material to the ZnO/TiO_2 heterostructure, it can be observed that it achieved the same RhB degradation (40 %) with equal UV exposure times. When compared to the ZnO material grown on office paper, a RhB degradation reduction to 40 % was observed if compared to the 51 % achieved by the pure material. In the case of the TiO_2 materials grown on Whatman paper, the RhB degradation reduction was more expressive (57 % of pure TiO_2 to 40 % of the heterostructure). These results indicate that the TiO_2 nanostructures (without acid) grown above ZnO could not effectively contribute to photocatalysis and in some extent interfering with the photocatalytic process. It is believed that the TiO_2 formed without acid has the anatase structure, as observed for the powder produced during heterostructure synthesis, with reduced size (see the broader peaks on **Figure A.4**). However, an incomplete conversion of phase can be expected for synthesis without acid, with effects on TiO_2 photocatalytic performance. Moreover, as reported in the literature, the acidic environment during the growth process of titanium dioxide nanoparticles is appropriate for the formation of well crystalline nanoparticles [103], and the lack of acid can result in amorphous materials [104].

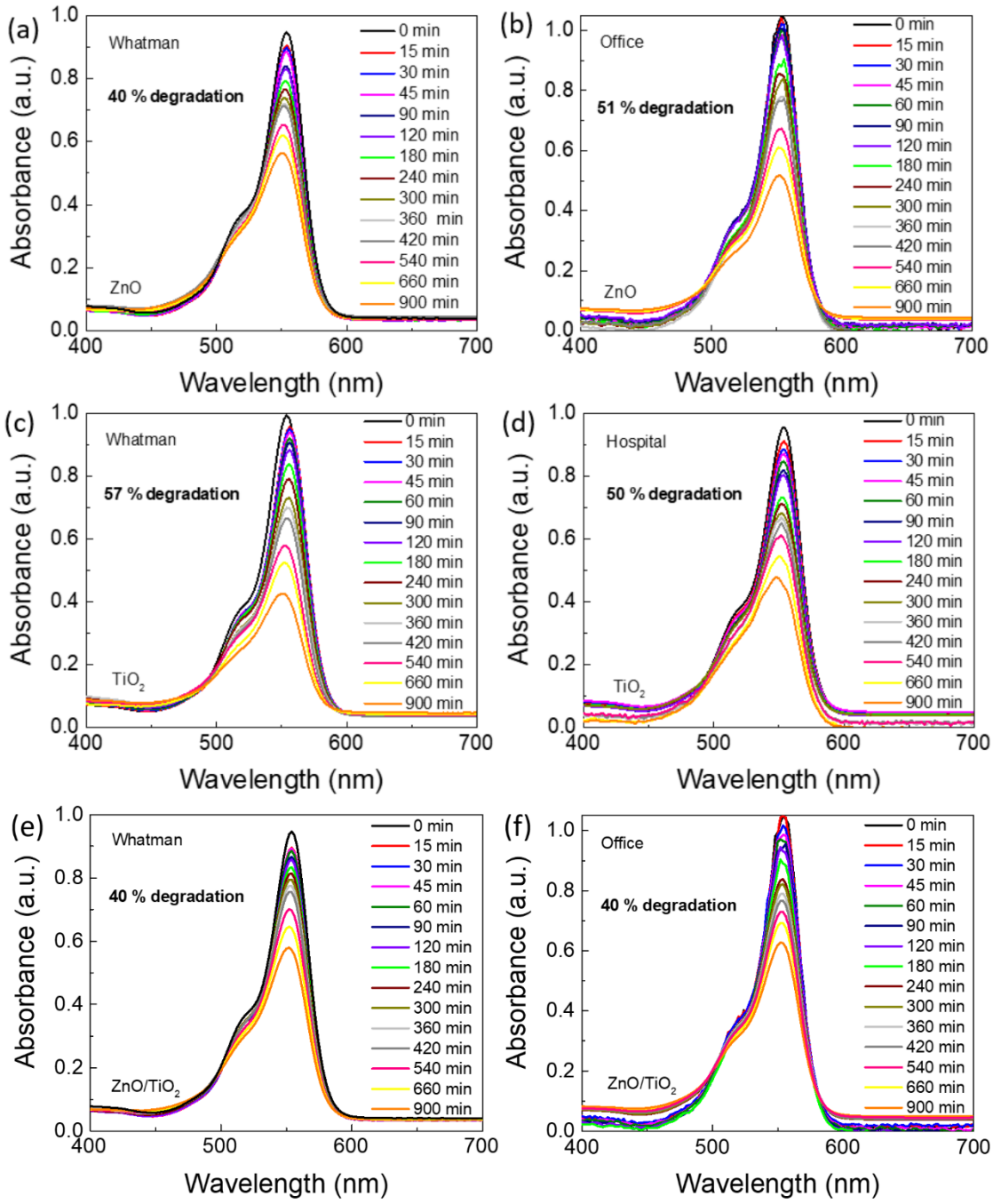

Figure 3.7 – RhB absorbance spectra under UV light exposures up to 15 h for ZnO nanostructures on (a) Whatman and (b) office papers; TiO_2 nanostructures (1 M, 30 min) grown on (c) Whatman and (d) hospital papers; and ZnO/TiO_2 heterostructures synthesized (e) without acid on Whatman and on (f) office papers. The measurements were carried out at room temperature.

The ZnO/TiO_2 heterostructure (25 mM) grown on office paper has also been investigated as photocatalyst. A RhB degradation of 50 % was obtained (**Figure 3.8**), and in the previous case (without acid) it was 40 % after 15 h of exposure time. The presence of acid even in smaller concentration can be responsible for the better TiO_2 performance, and when associated to the chemical etching of ZnO (structure modification), could have contributed to the overall enhanced photocatalytic activity. The holes and deterioration of the plate surface with laminar structures

observed in **Figure 3.3 (d)** is expected to have higher surface area, and thus more active sites will have been available for the dye molecules to react with the catalyst [58].

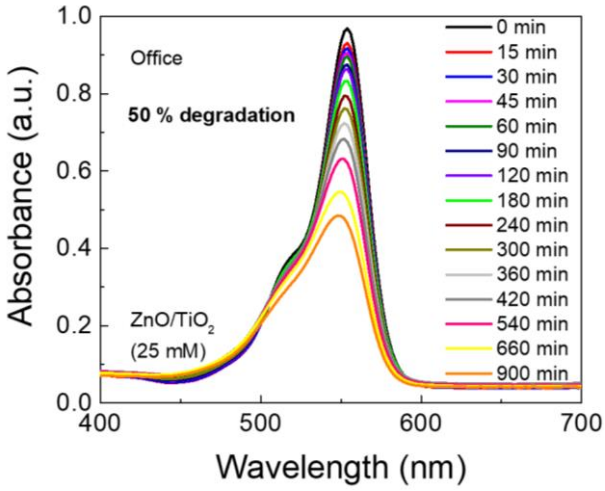

Figure 3.8 – RhB absorbance spectra under UV light exposure at room temperature up to 15 h for the ZnO/TiO_2 heterostructure (25 mM, 15 min) grown on office paper.

The degradation ratio (C/C_0) vs UV/solar light exposure time is presented in **Figure 3.9**, in which C is the absorbance of the RhB solution for each exposure time and C_0 is the initial solution absorbance [7]. A blank solution of rhodamine B was also exposed to solar/UV radiations. It has been observed that the blank solution was not influenced in both cases, and it can be concluded that the photocatalytic activity was only influenced by the catalyst. From **Figure 3.9**, it can be observed that under solar and UV radiations, the TiO_2 nanostructures grown on Whatman paper (1 M and 30 min synthesis time) had the highest photocatalytic activity among the materials investigated.

All these photocatalytic experiments open to the production of smart photocatalytic papers capable of decomposing organic pollutants when light-activated, even under solar radiation. The idea is to produce one-use materials, that are biocompatible, flexible and thus can be adapted to several surfaces, disposable and that can be easily recycled. Moreover, the approach developed in this study revealed to be clean, as no powder or extra processes have been used during photocatalysis, and environmentally friendly as photocatalysts, such as ZnO and TiO_2 that have been employed.

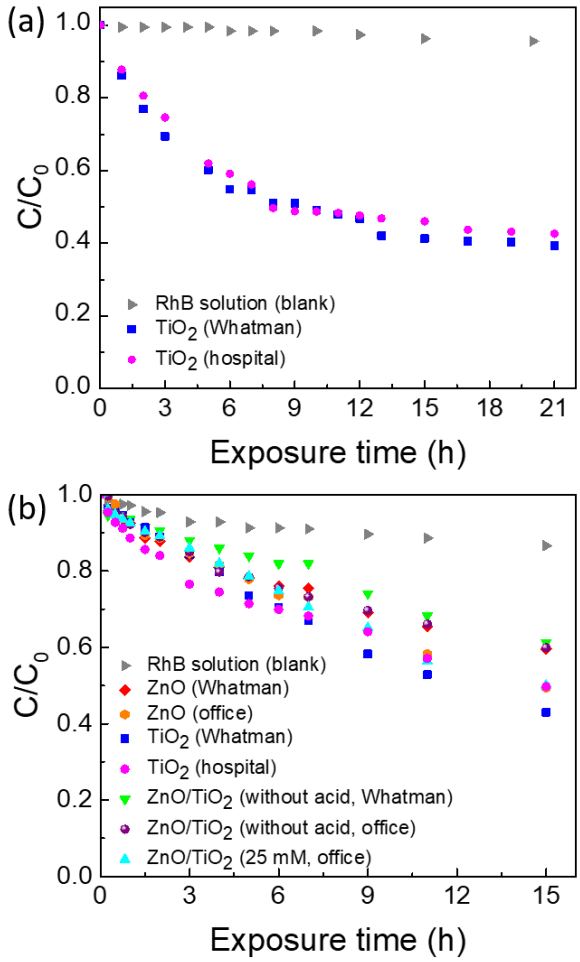

Figure 3.9 – (a) RhB degradation ratio (C/C_0) *vs* solar light exposure time and (b) RhB degradation ratio (C/C_0) *vs* UV exposure time.

3.4 UV sensing

Both zinc oxide and TiO_2 are highly sensitive to adsorption and desorption of gases due to oxygen vacancies on the surface [7,34]. Regarding the sensing mechanism, with no UV exposure (in the dark) and upon oxidation, the oxygen molecules adsorb to the surface of the semiconductors (ZnO or TiO_2) and accept free electrons leading to an electron reduction from the conduction band. As a result, the conductivity decreases. When the semiconductors are exposed to UV radiation, electron-hole pairs are generated when the incident photon energy is higher that their bandgap and holes migrate to the surface accelerated by a potential slope. This potential slope is produced by band bending and the negatively charged absorbed oxygen molecules are discharged under electron-hole recombination. As a consequence, oxygen is desorbed from the surface and the conductivity of the semiconductor increases [34,105]. In the present study, ZnO and TiO_2 nanostructures grown on Whatman, hospital and office papers have been tested as UV sensors. The ZnO/TiO_2 heterostructures were not investigated as UV sensors. Regarding the used substrates, hospital and office paper difficulted the production process of the sensors due to the porosity of the cellulose fibers, higher roughness and presence of impurities ($CaCO_3$). Whatman

paper, on the other hand, has been previously reported as substrate for UV sensors, and in this study, was also used for such devices. TiO_2 grown on Whatman paper did not behave as an UV sensor, and the most likely reason is the lack of seed layer below the nanostructures that would produce a continuous film, avoiding any current loss. The ZnO NRs grown on Whatman paper was the only condition that demonstrated a consistent UV sensing behavior, so the results of other materials were not presented in this study.

In the case of ZnO, the nanorod arrays grown on Whatman paper were successfully employed as UV sensors. The time resolved photocurrent of ZnO nanorod paper UV sensor is presented in **Figure 3.10**.

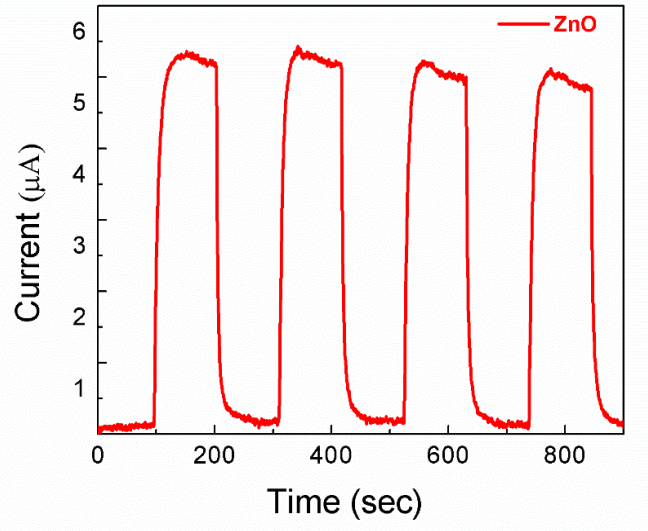

Figure 3.10 – ZnO-based UV sensor (80 °C, 15 min) on Whatman paper with carbon contacts impressed by screen-printing.

In **Figure 3.10**, it is possible to observe that the photocurrent exponentially increased from 0.10 µA to 5.0 µA (bias voltage of +10 V) and then decreased to its original value in approximately 109 s after the UV radiation was turned off. The photocurrent of ZnO UV sensors was completely reproducible during several cycles of photocurrent switching. The responsivity was calculated according to the following equation [7]:

$$R = \frac{I_{ph} - I_{dark}}{P_{UV}} \tag{3.2}$$

where I_{ph} is the UV sensor photocurrent, I_{dark} is the UV sensor dark current and P_{UV} is the power of the UV source [34]. Based on equation (3.2), the obtained responsivity value was 0.61 µA/W. For the responsivity it was taken into account the current value when the sensor reaches 95% of its stable value [9]. This value is almost 2 times lower than the one obtained in [9] (1.19 µA/W), however a lower temperature was used in the present study. According to the literature, higher temperatures lead to a better coverage of the substrate with nanorods as they become higher in length and well aligned. An increase in length leads to a higher aspect ratio of length to diameter which increases the sensitivity and responsivity [9].

3.5 Antibacterial activity: absorption method

The prevention of infections due to microorganisms is crucial in many sectors, for instance in healthcare, food/military industries and in water treatment [106]. Metal oxide nanostructures are widely used as antimicrobial agents [76], and the photocatalytic activity of TiO_2 has been extensively studied over the years and against a wide range of bacteria strains. However, the nanomaterials' mechanisms to inactivate the microorganisms are still under debate [106,107]. Several studies suggest that the high antibacterial activity of TiO_2 nanoparticles, when photoactivated, is mainly due to the peroxidation of the polyunsaturated phospholipids of the lipid membrane. However, it has been reported that a UV-light exposure with shorter wavelengths (UV-C and UV-B) leads to a faster and more efficient antimicrobial TiO_2 effect [18,19]. In terms of the substrate, hospital paper coming as coach rolls are largely used nowadays, and thus this approach can contribute to avoid proliferation of bacteria, while maintaining the low-cost and abundancy aspects of the material.

S. aureus are gram-positive abundant skin-colonizing bacteria and a very important cause of both nosocomial infections and community-associated skin infections [76,78]. The antibacterial activity of TiO_2 nanostructures grown on hospital paper (1 M, 15 min synthesis time) against this bacteria was quantitatively assessed accordingly to the equation (3.3) [28]:

$$A = (\log C_T - \log C_O) - (\log T_T - \log T_O) \quad (3.3)$$

where A is the value of the antibacterial activity, $\log C_T$, $\log C_0$, $\log T_T$, $\log T_O$ are the common logarithm of the average number of CFU obtained with control (C) and nanoparticle impregnated samples (T), respectively, immediately after inoculation (C_0 and T_0) and after the 18 h incubation (C_T and T_T). To evaluate the effectiveness of the assay on the materials, a classification is attributed and if $2 \leq A < 3$, the antibacterial properties are significant or if $A \geq 3$, they are strong [28,79].

The results showed that after 18 h of incubation, the control paper supported the growth of *S. aureus*. The obtained value for the antibacterial activity was 2.04. This value indicates significant TiO_2 antibacterial properties and means that, after inoculation and incubation, the logarithm of the number of bacteria in hospital paper functionalized with nanoparticles was 2.04 times lower than in control. The present results demonstrated that the investigated material has a satisfactory antibacterial activity, and with more investigation and development, these materials can be produced in large scale and evolve into the hospital environment, maintaining their low-cost characteristics.

4. Conclusion and future perspectives

ZnO and TiO_2 nanostructures, as well as ZnO/TiO_2 heterostructures were synthesized under microwave irradiation at low temperatures (80 °C), using synthesis times up to 30 min. Low-cost Whatman, office and hospital paper substrates were used. The synthesized materials were integrated on different applications namely photocatalysis, UV sensors and antimicrobial agents. Microwave synthesis successfully covered the substrates with the nanostructures in all conditions studied. ZnO nanoplates originating nano-flower structures on office paper were observed possibly due to the interaction between the calcium carbonate impurities and zinc. On Whatman and hospital papers, continuous ZnO nanorod arrays were observed. TiO_2 nanoparticles were successfully produced with oxalic acid and their size was highly influenced by the synthesis microwave time and the type of paper substrate used. XRD results showed the presence of pure ZnO wurtzite on Whatman paper. However, the identification of TiO_2 phase was only possible by using its powders collected after TiO_2 microwave syntheses. Anatase phase was obtained, which is believed to be the same crystalline phase of TiO_2 films on paper. Since the films have a low thickness (some nanometers), another technique could be employed to determine the phase of TiO_2 above the substrates, that is XPS (X-ray photoelectron spectroscopy).

The photocatalytic activity of the materials was assessed from rhodamine B degradation and the highest photocatalytic activity was obtained with pure TiO_2 nanostructures grown on Whatman paper, both under solar and UV radiations. The presence of dense agglomerates forming thick TiO_2 film layers on Whatman paper, as well as the ZnO nanoplates with high surface area on office paper may have contributed to the degradation of the pollutant in photocatalysis experiments. For the heterostructure (ZnO/TiO_2 without acid) on Whatman paper, agglomerates of TiO_2 were observed heterogeneously dispersed and their incomplete conversion of phase could have compromised the photocatalytic activity. In spite of the ZnO nanorods etching observed due to the oxalic acid (25 mM) in the heterostructure ZnO/TiO_2, the deterioration/higher surface area of the plates, on office paper, lead to a better photocatalytic activity under UV light.

Also, in photocatalysis reuse tests should be performed to confirm if the degradation percentage values do not modify with subsequent exposures. If a degradation reduction is observed, tests to check the adsorption of RhB molecules on paper, for instance by Reflectance IR spectroscopy have to be carried out.

The improvement of the heterostructure should be investigated in the next studies, since it is a promising photocatalyst. Not only the efficiency, but also the shift of absorption range to the visible is crucial. The microwave parameters should be adjusted, as well as the molar ratio of the acid which affects the particle size distribution, crystallinity, morphology and stability.

Furthermore, these nanoplatforms should maintain its cost effectiveness and as reported, cellulose-based substrates are a good alternative.

A ZnO-based UV sensor was fabricated on Whatman paper, demonstrating good responsivity and reproducibility during more than four tested cycles. The low thickness of TiO_2 films combined with the roughness of cellulose fibers may have contributed to the current loss and non-functional devices. To avoid this problem, a TiO_2 seed layer could be tested in the future.

TiO_2 nanostructures grown on hospital paper demonstrated significant antibacterial activity against *Staphylococcus aureus* and the use of titanium dioxide on this type of paper can be particularly attractive and an alternative for fighting the proliferation of bacteria, especially in hospital environments. Despite of being a qualitative test, the most used antibacterial assay reported in the literature is Kirby-Bauer. To compare results, in addition to the absorption method, Kirby-Bauer could also be tested in future works. Some studies demonstrated the potent antimicrobial activity by using isolated nanostructures and better antibacterial activity was achieved when ZnO and TiO_2 were combined. As a conclusion, a possible enhancement of the antibacterial activity could be obtained with the heterostructure (ZnO/TiO_2), and further researches should be performed in this area, focusing on assays under visible light and on disposable low-cost substrates, such as hospital paper.

Another suggestion for future works is the synthesis of TiO_2 nanorods followed by the deposition of a uniform ZnO layer of nanostructures *e.g.* nanoparticles. The aim is to obtain a TiO_2/ZnO heterostructure by the hydrothermal method assisted by microwave irradiation on paper. The achieved nanoplatforms should afterwards be studied as photocatalysts, antibacterial agents and UV sensors.

In summary, it was demonstrated that ZnO and TiO_2 nanostructures can be effectively produced with a fast and inexpensive microwave irradiation approach on different cellulose-based substrates creating functionalized papers that can be further adapted and selected to multifunctional applications.

(A research article was developed based on this master's thesis titled "Paper-based nanoplatforms for multifunctional applications" to be published in *Journal of Nanomaterials.*)

References

[1] D. Nunes, A. Pimentel, L. Santos, P. Barquinha, E. Fortunato, R. Martins, "Photocatalytic TiO_2 Nanorod Spheres and Arrays Compatible with Flexible Applications", *Catalysts*. 7 (2017) 60.

[2] D. Nunes, A. Pimentel, J. V. Pinto, T.R. Calmeiro, S. Nandy, P. Barquinha, L. Pereira, P.A. Carvalho, E. Fortunato, R. Martins, "Photocatalytic behavior of TiO_2 films synthesized by microwave irradiation", *Catalysis Today*. 278 (2016) 262–270. doi:10.1016/j.cattod.2015.10.038.

[3] D. Mora-Fonz, T. Lazauskas, M.R. Farrow, C.R.A. Catlow, S.M. Woodley, A.A. Sokol, "Why Are Polar Surfaces of ZnO Stable?", *Chemistry of Materials*. 29 (2017) 5306–5320.

[4] S. Johari, N.Y. Muhammad, M.R. Zakaria, "Study of zinc oxide thin film characteristics", *EPJ Web of Conferences*. 162 (2017) 1–4. doi:10.1051/epjconf/201716201057.

[5] A. Pimentel, D. Nunes, P. Duarte, J. Rodrigues, F.M. Costa, T. Monteiro, R. Martins, E. Fortunato, "Synthesis of long ZnO nanorods under microwave irradiation or conventional heating", *Journal of Physical Chemistry C*. 118 (2014) 14629–14639. doi:10.1021/jp5027509.

[6] A. Pimentel, D. Nunes, S. Pereira, R. Martins, E. Fortunato, "Photocatalytic Activity of TiO_2 Nanostructured Arrays Prepared by Microwave-Assisted Solvothermal Method", *IntechOpen*, Chapter 3, 2016. doi:10.5772/63237.

[7] D. Nunes, A. Pimentel, A. Araujo, T.R. Calmeiro, S. Panigrahi, J.V. Pinto, P. Barquinha, M. Gama, E. Fortunato, R. Martins, "Enhanced UV Flexible Photodetectors and Photocatalysts Based on TiO_2 Nanoplatforms", *Springer Nature*, (2018) 1–16. doi:10.1007/s11244-018-0968-4.

[8] A. Pimentel, A. Araújo, B. Coelho, D. Nunes, M. Oliveira, M. Mendes, H. Águas, R. Martins, E. Fortunato, "3D ZnO/Ag Surface-Enhanced Raman Scattering on Disposable and Flexible Cardboard Platforms", *Materials*. 10 (2017). doi:10.3390/ma10121351.

[9] A. Pimentel, A. Samouco, D. Nunes, A. Araújo, R. Martins, E. Fortunato, "Ultra-fast microwave synthesis of ZnO nanorods on cellulose substrates for UV sensor applications", *Materials*. 10 (2017) 1–18. doi:10.3390/ma10111308.

[10] N. D., K.K. Kondamareddy, H. Bin, D. Lu, P. Kumar, R.K. Dwivedi, V.O. Pelenovich, X.-Z. Zhao, W. Gao, D. Fu, "Enhanced visible light photodegradation activity of RhB/MB from aqueous solution using nanosized novel Fe-Cd co-modified ZnO", *Scientific Reports*. 8 (2018) 10691. doi:10.1038/s41598-018-29025-1.

[11] P. Gonçalves, R. Bertholdo, J.A. Dias, S. Carvalho Maestrelli, T.R. Giraldi, "Evaluation of the Photocatalytic Potential of TiO_2 and ZnO Obtained by Different Wet Chemical Methods", *Materials Research*. 20 (2017) 181–189.

[12] R. Goyay, D. Kishore, "Investigation of Photocatalytic Degradation of Rhodamine B by Using Nano-Sized TiO_2", *IJSRM*. 5 (2017) 6006–6013. doi:10.18535/ijsrm/v5i7.25.

[13] S. Nihalani, A. Vijay, S. Bhardwaj, "Removal of contaminants from industrial effluents using nano

photocatalyst $BaO_3TiO.SrO_3TiO$", *Indian Journal of Chemical Technology*, 23 (2016) 437–441.

[14] B. Barrocas, O.C. Monteiro, M.E.M. Jorge, S. Sério, "Photocatalytic activity and reusability study of nanocrystalline TiO_2 films prepared by sputtering technique", *Applied Surface Science*. 264 (2013) 111–116. doi:10.1016/j.apsusc.2012.09.136.

[15] X.X. Ou, C. Wang, Y. Su, F.J. Zhang, G.J. Yang, L.Y. Wang, "Degradation of Rhodamine B in aqueous solution by the UV/ZnO photocatalytic process", *Advanced Materials Research*. 233–235 (2011) 737–740.

[16] S.P. Ghosh, K.C. Das, N. Tripathy, G. Bose, D.H. Kim, T.I. Lee, J.M. Myoung, J.P. Kar, "Ultraviolet photodetection characteristics of Zinc oxide thin films and nanostructures", *IOP Conf. Series: Materials Science and Engineering.* 115 (2016). doi:10.1088/1757-899X/115/1/012035.

[17] A. Sirelkhatim, S. Mahmud, A. Seeni, N.H.M. Kaus, L.C. Ann, S.K.M. Bakhori, H. Hasan, D. Mohamad, "Review on zinc oxide nanoparticles: Antibacterial activity and toxicity mechanism", *Nano-Micro Letters.* 7 (2015) 219–242. doi:10.1007/s40820-015-0040-x.

[18] U. Joost, K. Juganson, M. Visnapuu, M. Mortimer, A. Kahru, E. Nõmmiste, U. Joost, V. Kisand, A. Ivask, "Photocatalytic antibacterial activity of nano-TiO_2 (anatase)-based thin films: Effects on *Escherichia coli* cells and fatty acids", *Journal of Photochemistry and Photobiology B: Biology*. 142 (2015) 178–185.

[19] R.J. Barnes, R. Molina, J. Xu, P.J. Dobson, I.P. Thompson, "Comparison of TiO_2 and ZnO nanoparticles for photocatalytic degradation of methylene blue and the correlated inactivation of gram-positive and gram-negative bacteria", *Journal of Nanoparticle Research*. 15 (2013). doi:10.1007/s11051-013-1432-9.

[20] E.M.C. Fortunato, P.M.C. Barquinha, A.C.M.B.G. Pimentel, A.M.F. Gonçalves, A.J.S. Marques, L.M.N. Pereira, R.F.P. Martins, "Fully transparent ZnO thin-film transistor produced at room temperature", *Advanced Materials*. 17 (2005) 590–594. doi:10.1002/adma.200400368.

[21] P.F. Carcia, R.S. McLean, M.H. Reilly, G. Nunes, "Transparent ZnO thin-film transistor fabricated by rf magnetron sputtering", *Applied Physics Letters*. 82 (2003) 1117–1119. doi:10.1063/1.1553997.

[22] S. Panigrahi, T. Calmeiro, R. Martins, D. Nunes, E. Fortunato, "Observation of Space Charge Dynamics Inside an All Oxide Based Solar Cell", *ACS Nano*. 10 (2016) 6139–6146. doi:10.1021/acsnano.6b02090.

[23] I. Repins, M.A. Contreras, B. Egaas, C. DeHart, J. Scharf, C.L. Perkins, B. To, R. Noufi, "19·9%-efficient ZnO/CdS/$CuInGaSe^2$ solar cell with 81·2% fill factor", *Progress in Photovoltaics: Research and Applications*. 16 (2008) 235–239. doi:10.1002/pip.822.

[24] A. Pimentel, J. Rodrigues, P. Duarte, D. Nunes, F.M. Costa, T. Monteiro, R. Martins, E. Fortunato, "Effect of solvents on ZnO nanostructures synthesized by solvothermal method assisted by microwave radiation: a photocatalytic study", *Journal of Materials Science.* 50 (2015) 5777–5787. doi:10.1007/s10853-015-9125-7.

[25] X. Zong, R. Zhu, "ZnO nanorod-based FET biosensor for continuous glucose monitoring", *Sensors and Actuators, B: Chemical*. 255 (2018) 2448–2453. doi:10.1016/j.snb.2017.09.037.

[26] K.M. Lee, C.W. Lai, K.S. Ngai, J.C. Juan, "Recent developments of zinc oxide based photocatalyst in water treatment technology: A review", *Water Research*. 88 (2015) 428–448. doi:doi: 10.1016/j.watres.2015.09.045.

[27] J.O. Carneiro, A.P. Samantilleke, P. Parpot, F. Fernandes, M. Pastor, A. Correia, E.A. Luís, A.A. Chivanga Barros, V. Teixeira, "Visible Light Induced Enhanced Photocatalytic Degradation of Industrial Effluents (Rhodamine B) in Aqueous Media Using TiO_2 Nanoparticles", *Journal of Nanomaterials*. (2016) 1–13. doi:10.1155/2016/4396175.

[28] R. Borda d' Água, R. Branquinho, M.P. Duarte, E. Maurício, A.L. Fernando, R. Martins, E. Fortunato, "Efficient coverage of ZnO nanoparticles on cotton fibres for antibacterial finishing using a rapid and low cost *in situ* synthesis", *New Journal of Chemistry*. 42 (2018) 1052–1060. doi:10.1039/C7NJ03418K.

[29] P. Dao, "Fabrication and Properties of 1-Dimensional TiO_2 and ZnO Nanocomposites Prepared by Hydrothermal Method", University College of Southeast Norway, 2016.

[30] M. Niskanen, M. Kuisma, O. Cramariuc, V. Golovanov, T.I. Hukka, N. Tkachenko, T.T. Rantala, "Porphyrin adsorbed on the (1010) surface of the wurtzite structure of ZnO-conformation induced effects on the electron transfer characteristics", *Physical Chemistry Chemical Physics*. 15 (2013) 17408–17418.

[31] H. Morkoc, U. Ozgur, "Zinc Oxide: Fundamentals, Materials and Device Technology", 1st ed., Chapter 1, *Wiley-VCH*, 2009.

[32] V. Coleman, C. Jagadish, "Zinc oxide bulk, thin films and nanostructures : processing, properties and applications", 1st ed., *Oxford: Elsevier Science*, 1-20, 2006.

[33] G.C. Yi, C. Wang, W. Park, "ZnO nanorods: synthesis, characterization and applications", *Semiconductor Science and Technology*. 20 (2005) S22–S34. doi:10.1088/0268-1242/20/4/003.

[34] A. Pimentel, S.H. Ferreira, D. Nunes, T. Calmeiro, R. Martins, E. Fortunato, "Microwave synthesized ZnO nanorod arrays for UV sensors: A seed layer annealing temperature study", *Materials*. 9 (2016). doi:10.3390/ma9040299.

[35] M. Pavan, S. Rühle, A. Ginsburg, D.A. Keller, H.N. Barad, P.M. Sberna, D. Nunes, R. Martins, A.Y. Anderson, A. Zaban, E. Fortunato, "TiO_2/Cu_2O all-oxide heterojunction solar cells produced by spray pyrolysis", *Solar Energy Materials and Solar Cells*. 132 (2015) 549–556.

[36] K. Kardarian, D. Nunes, P. Maria Sberna, A. Ginsburg, D.A. Keller, J. Vaz Pinto, J. Deuermeier, A.Y. Anderson, A. Zaban, R. Martins, E. Fortunato, "Effect of Mg doping on Cu_2O thin films and their behavior on the TiO_2/Cu_2O heterojunction solar cells", *Solar Energy Materials and Solar Cells*. 147 (2016) 27–36.

[37] N.G. Park, G. Schlichthörl, J. Van De Lagemaat, H.M. Cheong, A. Mascarenhas, A.J. Frank, "Dye-sensitized TiO_2 solar cells: Structural and photoelectrochemical characterization of nanocrystalline electrodes formed from the hydrolysis of $TiCl_4$, *Journal of Physical Chemistry B*. 103 (1999) 3308–3314. doi:10.1021/jp984529i.

[38] B. O'Regan, M. Grätzel, "A low-cost, high-efficiency solar cell based on dye-sensitized colloidal TiO_2 films", *Nature*. 353 (1991) 737–740. doi:10.1038/353737a0.

[39] K. Nakata, A. Fujishima, "TiO_2 photocatalysis: Design and applications", *Journal of Photochemistry and Photobiology C: Photochemistry Reviews*. 13 (2012) 169–189.

[40] S. Sério, M.E. Melo Jorge, M.L. Coutinho, S.V. Hoffmann, P. Limão-Vieira, Y. Nunes, "Spectroscopic studies

of anatase TiO_2 thin films prepared by DC reactive magnetron sputtering", *Chemical Physics Letters*. 508 (2011) 71–75. doi:10.1016/j.cplett.2011.04.002.

[41] C.L. Bianchi, C. Pirola, M. Stucchi, B. Sacchi, G. Cerrato, S. Morandi, A. Di Michele, A. Carletti, V. Capucci, "A New Frontier of Photocatalysis Employing Micro-Sized TiO_2: Air/Water Pollution Abatement and Self-Cleaning/ Antibacterial Applications", *IntechOpen*, Chapter 23, 2016. doi:10.5772/62892.

[42] U. Diebold, "The surface science of titanium dioxide", *Surface Science Reports*. 48 (2003) 53–229. doi:10.1016/S0167-5729(02)00100-0.

[43] R. Kaplan, B. Erjavec, G. Dražić, J. Grdadolnik, A. Pintar, "Simple synthesis of anatase/rutile/brookite TiO_2 nanocomposite with superior mineralization potential for photocatalytic degradation of water pollutants", *Applied Catalysis B: Environmental.* 181 (2016) 465–474. doi:10.1016/j.apcatb.2015.08.027.

[44] V. Etacheri, C. Di Valentin, J. Schneider, D. Bahnemann, S. C.Pillai, "Visible-light activation of TiO_2 photocatalysts: Advances in theory and experiments", *Journal of Photochemistry and Photobiology C: Photochemistry Reviews*. 25 (2015) 1–29.

[45] C. Byrne, R. Fagan, S. Hinder, D.E. McCormack, S.C. Pillai, "New approach of modifying the anatase to rutile transition temperature in TiO_2 photocatalysts", *RSC Advances*. 6 (2016) 95232–95238.

[46] A. Di Paola, M. Bellardita, L. Palmisano, "Brookite, the Least Known TiO_2 Photocatalyst," *Catalysts*. 3 (2013) 36–73. doi:10.3390/catal3010036.

[47] B.I. Lee, X. Wang, R. Bhave, M. Hu, "Synthesis of brookite TiO_2 nanoparticles by ambient condition sol process", *Materials Letters*. 60 (2006) 1179–1183.

[48] Y. Lan, Y. Lu, Z. Ren, "Mini review on photocatalysis of titanium dioxide nanoparticles and their solar applications", *Nano Energy*. 2 (2013) 1031–1045. doi:10.1016/j.nanoen.2013.04.002.

[49] T. Luttrell, S. Halpegamage, J. Tao, A. Kramer, E. Sutter, M. Batzill, "Why is anatase a better photocatalyst than rutile? - Model studies on epitaxial TiO_2 films", *Scientific Reports*. 4 (2015) 4043. doi:10.1038/srep04043.

[50] K. Fischer, A. Gawel, D. Rosen, M. Krause, A. Abdul Latif, J. Griebel, A. Prager, A. Schulze, "Low-Temperature Synthesis of Anatase/Rutile/Brookite TiO_2 Nanoparticles on a Polymer Membrane for Photocatalysis", *Catalysts*. 7 (2017) 209. doi:10.3390/catal7070209.

[51] R. Boppella, P. Basak, S. V Manorama, "Viable Method for the Synthesis of Biphasic TiO_2 Nanocrystals with Tunable Phase Composition and Enabled Visible-Light Photocatalytic Performance", *ACS Appl. Mater. Interfaces.* 4 (2012) 1239–1246. doi:10.1021/am201354r.

[52] D. Reyes-Coronado, G. Rodríguez-Gattorno, M.E. Espinosa-Pesqueira, C. Cab, R. De Coss, G. Oskam, "Phase-pure TiO_2 nanoparticles: Anatase, brookite and rutile", *Nanotechnology*. 19 (2008) 1–10. doi:10.1088/0957-4484/19/14/145605.

[53] D. Nunes, L. Santos, A. Pimentel, P. Barquinha, L. Pereira, E. Fortunato, R. Martins, "Metal Oxide Nanostructures: Synthesis, Properties and Applications", 1st ed., *Elsevier*, 2018.

[54] H.Y. Xu, H. Wang, Y.C. Zhang, W.L. He, M.K. Zhu, B. Wang, H. Yan, "Hydrothermal synthesis of zinc oxide powders with controllable morphology", *Ceramics International*. 30 (2004) 93–97. doi:10.1016/S0272-8842(03)00069-5.

[55] Y. Li, M. Guo, M. Zhang, X. Wang, "Hydrothermal synthesis and characterization of TiO_2 nanorod arrays on glass substrates", *Materials Research Bulletin*. 44 (2009) 1232–1237. doi:10.1016/j.materresbull.2009.01.009.

[56] H. Yin, Y. Wada, T. Kitamura, S. Kambe, S. Murasawa, H. Mori, T. Sakata, S. Yanagida, "Hydrothermal synthesis of nanosized anatase and rutile TiO_2 using amorphous phase TiO_2", *Journal of Materials Chemistry*. 11 (2001) 1694–1703. doi:10.1039/b008974p.

[57] B.L. And, H.C. Zeng, "Hydrothermal Synthesis of ZnO Nanorods in the Diameter Regime of 50 nm", *J. Am. Chem. Soc.* 125 (15) (2003) 4430–4431. doi:10.1021/ja0299452.

[58] A.B. Djurišić, Y.H. Leung, A.M. Ching Ng, "Strategies for improving the efficiency of semiconductor metal oxide photocatalysis", *Materials Horizons*. 1 (2014) 400. doi:10.1039/c4mh00031e.

[59] Z.R. Ismagilov, L.T. Tsikoza, N. V Shikina, V.F. Zarytova, V. V Zinoviev, S.N. Zagrebelnyi, "Synthesis and stabilization of nano-sized titanium dioxide", *Russian Chemical Reviews*. 78 (2009) 873–885. doi:10.1070/RC2009v078n09ABEH004082.

[60] A.T. Vicente, A. Araújo, D. Gaspar, L. Santos, A.C. Marques, M.J. Mendes, L. Pereira, E. Fortunato, R. Martins, "Optoelectronics and Bio Devices on Paper Powered by Solar Cells", *IntechOpen*, Chapter 3, 2017. doi:10.5772/66695.

[61] A. T. Vicente, A. Araújo, M.J. Mendes, D. Nunes, M.J. Oliveira, O. Sanchez-Sobrado, M.P. Ferreira, H. Águas, E. Fortunato, R. Martins, "Multifunctional cellulose-paper for light harvesting and smart sensing applications", *Journal of Materials Chemistry C*. 6 (2018) 3143–3181. doi:10.1039/C7TC05271E.

[62] R. Martins, D. Gaspar, M. J. Mendes, L. Pereira, J. Martins, P. Bahubalindruni, P. Barquinha, E. Fortunato, "Papertronics: Multigate paper transistor for multifunction applications", *Applied Materials Today*. 12 (2018) 402–414.

[63] R. Fagan, D.E. McCormack, D.D. Dionysiou, S.C. Pillai, "A review of solar and visible light active TiO_2 photocatalysis for treating bacteria, cyanotoxins and contaminants of emerging concern", *Materials Science in Semiconductor Processing*. 42 (2016) 2–14. doi:10.1016/j.mssp.2015.07.052.

[64] K. Kalyanasundaram, "Photochemical applications of solar energy: photocatalysis and photodecomposition of water", *The Royal Society of Chemistry: Photochemistry*. (2013) 182–265. doi:10.1039/9781849737722-00182.

[65] M.M. Khan, S.F. Adil, A. Al-Mayouf, "Metal oxides as photocatalysts", *Journal of Saudi Chemical Society*. (2015). doi:10.1016/j.jscs.2015.04.003.

[66] J. Zhang, S. Yan, L. Fu, F. Wang, M. Yuan, G. Luo, Q. Xu, X. Wang, C. Li, "Photocatalytic Degradation of Rhodamine B on Anatase, Rutile, and Brookite TiO_2", *Chinese Journal of Catalysis*. 32 (2011) 983–991. doi:10.1016/S1872-2067(10)60222-7.

[67] J.M. Chem, B. Liu, Z. Wang, Y. Dong, Y. Zhu, Y. Gong, S. Ran, Z. Liu, J. Xu, Z. Xie, D. Chen, G. Shen, "ZnO-nanoparticle-assembled cloth for flexible photodetectors and recyclable photocatalysts", *Journal of Materials Chemistry*. 22 (2012) 9379–9384. doi:10.1039/c2jm16781f.

[68] E.S. Araújo, B.P. da Costa, R.A.P. Oliveira, J. Libardi, P.M. Faia, H.P. de Oliveira, "TiO_2 /ZnO hierarchical heteronanostructures: Synthesis, characterization and application as photocatalysts", *Journal of Environmental Chemical Engineering*. 4 (2016) 2820–2829. doi:10.1016/j.jece.2016.05.021.

[69] T. Bora, P. Sathe, K. Laxman, S. Dobretsov, J. Dutta, "Defect engineered visible light active ZnO nanorods for photocatalytic treatment of water", *Catalysis Today*. 284 (2017) 11–18. doi:10.1016/j.cattod.2016.09.014.

[70] J. Zhang, B. Wu, L. Huang, P. Liu, X. Wang, Z. Lu, G. Xu, E. Zhang, H. Wang, Z. Kong, J. Xi, Z. Ji, "Anatase nano-TiO_2 with exposed curved surface for high photocatalytic activity", *Journal of Alloys and Compounds.* 661 (2016) 441–447. doi:10.1016/j.jallcom.2015.11.225.

[71] B. İkizler, S.M. Peker, "Synthesis of TiO_2 coated ZnO nanorod arrays and their stability in photocatalytic flow reactors", *Thin Solid Films.* 605 (2016) 232–242. doi:10.1016/j.tsf.2015.11.083.

[72] S. Panigrahi, D. Basak, "Core–shell TiO_2@ZnO nanorods for efficient ultraviolet photodetection", *Royal Society of Chemistry: Nanoscale*. 3 (2011) 2336. doi:10.1039/c1nr10064e.

[73] W. Kim, S. Kim, D. Yoo, E.J. Kim, S.H. Hahn, "Annealing Effect of ZnO Seed Layer on Enhancing Photocatalytic Activity of ZnO/TiO_2 Nanostructure", *International Journal of Photoenergy*. (2013) 1–7. doi:dx.doi.org/10.1155/2013/130541.

[74] R.G.S.V. Prasad, S.S. Sophee, J.V. Srinivas, R.S.L. Aparna, A.R. Phani, "Antibacterial Activity of TiO_2 and ZnO Microparticles Combination on Water Polluting Bacteria", *Journal of Green Science and Technology*. 1 (2012) 1–7. doi:10.1166/jgst.2013.1008.

[75] M. Altan, H. Yildirim, "Comparison of Antibacterial Properties of Nano TiO_2 and ZnO Particle Filled Polymers", *Acta Physica Polonica A*. vol. 125 (2014). doi:10.12693/APhysPolA.125.645.

[76] A. Jesline, N.P. John, P.M. Narayanan, C. Vani, S. Murugan, "Antimicrobial activity of zinc and titanium dioxide nanoparticles against biofilm-producing methicillin-resistant *Staphylococcus aureus*", *Applied Nanoscience*. 5 (2015) 157–162. doi:10.1007/s13204-014-0301-x.

[77] C. Jayaseelan, A.A. Rahuman, S.M. Roopan, A.V. Kirthi, J. Venkatesan, S.-K. Kim, M. Iyappan, C. Siva, "Biological approach to synthesize TiO_2 nanoparticles using *Aeromonas hydrophila* and its antibacterial activity", *Spectrochimica Acta Part A: Molecular and Biomolecular Spectroscopy*. 107 (2013) 82–89. doi:10.1016/j.saa.2012.12.083.

[78] S.J. Cavalieri, "Manual of antimicrobial susceptibility testing", *American Society for Microbiology*, 2005.

[79] R. Borda d'Água, "Desenvolvimento de técnicas de impregnação de nanopartículas de óxido de zinco de baixo custo com propriedades antimicrobianas em tecidos", FCT, UNL, 2015.

[80] T. Silhavy, D. Kahne, S. Walker, "The bacterial cell envelope", *Cold Spring Harbor Perspectives in Biology*. (2010) 1–16.

[81] Y. Xu, M.-T. Wei, H.D. Ou-Yang, S.G. Walker, H.Z. Wang, C.R. Gordon, S. Guterman, E. Zawacki, E. Applebaum, P.R. Brink, M. Rafailovich, T. Mironava, "Exposure to TiO_2 nanoparticles increases *Staphylococcus aureus* infection of HeLa cells", *Journal of Nanobiotechnology*. 14 (2016) 1–34. doi:10.1186/s12951-016-0184-y.

[82] C.A. Schneider, W.S. Rasband, K.W. Eliceiri, "NIH Image to ImageJ: 25 years of image analysis", *Nature Methods*. 9 (2012) 671–5.

[83] A.C. Alba-Rubio, J. Santamaría-González, J.M. Mérida-Robles, R. Moreno-Tost, D. Martín-Alonso, A. Jiménez-López, P. Maireles-Torres, "Heterogeneous transesterification processes by using CaO supported on zinc oxide as basic catalysts", *Catalysis Today*. 149 (2010) 281–287. doi:10.1016/j.cattod.2009.06.024.

[84] H.C. Hsu, C.I. Lin, H.K. Chen, "Zinc Recovery from Spent ZnO Catalyst by Carbon in the Presence of Calcium Carbonate", *Metallurgical and Materials Transactions B: Process Metallurgy and Materials Processing Science*. 35 (2004) 55–63. doi:10.1007/s11663-004-0096-3.

[85] A.R. Jamaludin, S.R. Kasim, Z.A. Ahmad, "The Effect of $CaCO_3$ Addition on Physical Properties of ZnO-based", *Advanced Materials Research.* 620 (2013) 12–16.

[86] Z.R. Tian, J.A. Voigt, J. Liu, B. Mckenzie, M.J. Mcdermott, "Biomimetic arrays of oriented helical ZnO nanorods and columns", *Journal of the American Chemical Society.* 124 (2002) 12954–12955. doi:10.1021/ja0279545.

[87] A.C. Marques, L. Santos, M.N. Costa, J.M. Dantas, P. Duarte, A. Gonçalves, R. Martins, C.A. Salgueiro, E. Fortunato, "Office paper platform for bioelectrochromic detection of electrochemically active bacteria using tungsten trioxide nanoprobes", *Scientific Reports.* 5 (2015) 1–7. doi:10.1038/srep09910.

[88] T. Yoshida, "Leaching of Zinc Oxide in Acidic Solution", *Materials Transactions*. 44 (2003) 2489–2493. doi:10.2320/matertrans.44.2489.

[89] J. Hüpkes, J.I. Owen, S.E. Pust, E. Bunte , "Chemical Etching of Zinc Oxide for Thin-Film Silicon Solar Cells", *ChemPhysChem*. 13 (2012) 66–73. doi:10.1002/cphc.201100738.

[90] C. Xu, J. Wang, Y. Wang, "Synthesis of ZnO Nanograins by Immersing Zn Powders in Oxalic Acid Solution Plus Thermal Decomposition", *Journal of Nanoscience and Nanotechnology*. 15 (2015) 10002–7.

[91] D. Sridevi, K. V Rajendran, "Synthesis and optical characteristics of ZnO nanocrystals", *Bull. Mater. Sci*. 32 (2009) 165–168.

[92] A. Aminzadeh, "Fluorescence bands in the FT-Raman spectra of some calcium minerals", *Spectrochimica Acta - Part A: Molecular and Biomolecular Spectroscopy*. 53 (1997) 693–697. doi:10.1016/S1386-1425(96)01848-3.

[93] S.N. White, "Laser Raman spectroscopy as a technique for identification of seafloor hydrothermal and cold seep minerals", *Chemical Geology*. 259 (2009) 240–252. doi:10.1016/j.chemgeo.2008.11.008.

[94] M.-C.C. Po-I Liu, Li-Ching Chung, Hsin Shao, Teh-Ming Liang, Ren-Yang Horng, M. M. Chen-Chi, "A Short Review: Synthesis of Anatase TiO_2 and Its Composite by Ionothermal System under Microwave Heating and

Their Water Treatment Applications", *Materials Science Research Journal*. 8 (2014) 271–292.

[95] Kunlun Ding, Zhenjiang Miao, Zhimin Liu, Zhaofu Zhang, Buxing Han, Guimin An, A. Shiding Miao, Y. Xie, "Facile Synthesis of High Quality TiO_2 Nanocrystals in Ionic Liquid via a Microwave-Assisted Process", *J. Am. Chem. Soc*. 129 (20) (2007) 6362–6363. doi:10.1021/ja070809c.

[96] A.V. Murugan, V. Samuel, V. Ravi, "Synthesis of nanocrystalline anatase TiO_2 by microwave hydrothermal method", *Materials Letters*. 60 (2006) 479–480.

[97] A. Fahmi, C. Minot, P. Fourré, P. Nortier, "A theoretical study of the adsorption of oxalic acid on TiO_2", *Surface Science*. 343 (1995) 261–272. doi:10.1016/0039-6028(95)00813-6.

[98] V. Srikant, D.R. Clarke, "On the optical band gap of zinc oxide", *Journal of Applied Physics*. 83 (1998) 5447–5451. doi:10.1063/1.367375.

[99] H. Razavi-Khosroshahi, K. Edalati, J. Wu, Y. Nakashima, M. Arita, Y. Ikoma, M. Sadakiyo, Y. Inagaki, A. Staykov, M. Yamauchi, Z. Horita, M. Fuji, "High-pressure zinc oxide phase as visible-light-active photocatalyst with narrow band gap", *Journal of Materials Chemistry A*. 5 (2017). doi:10.1039/c7ta05262f.

[100] A.S. Kristoffersen, S.R. Erga, B. Hamre, Ø. Frette, "Testing fluorescence lifetime standards using two-photon excitation and time-domain instrumentation: Rhodamine B, coumarin 6 and lucifer yellow", *Journal of Fluorescence*. 24 (2014) 1015–1024. doi:10.1007/s10895-014-1368-1.

[101] F. Chen, J. Zhao, H. Hidaka, "Highly selective deethylation of Rhodamine B: Adsorption and photooxidation pathways of the dye on the TiO_2/SiO_2 composite photocatalyst", *International Journal of Photoenergy*. 5 (2003) 209–217.

[102] A.A. Al-Kahtani, "Photocatalytic Degradation of Rhodamine B Dye in Wastewater Using Gelatin/CuS/PVA Nanocomposites under Solar Light Irradiation", *Journal of Biomaterials and Nanobiotechnology*. 08 (2017) 66–82. doi:10.4236/jbnb.2017.81005.

[103] R. Thapa, S. Maiti, T.H. Rana, U.N. Maiti, K.K. Chattopadhyay, "Anatase TiO_2 nanoparticles synthesis via simple hydrothermal route: Degradation of Orange II, Methyl Orange and Rhodamine B", *Journal of Molecular Catalysis A: Chemical*. 363–364 (2012) 223–229. doi:10.1016/j.molcata.2012.06.013.

[104] A. Gustavsson, "Solar Photocatalytic Degradation of Rhodamine B by TiO_2 Nanoparticle Composites", 2010 2–6.

[105] B.S. Witkowski, L. Wachnicki, S. Gieraltowska, P. Sybilski, K. Kopalko, M. Stachowicz, M. Godlewski, "UV detector based on zinc oxide nanorods obtained by the hydrothermal method", *Physica Status Solidi (C)*. 11 (2014) 1447–1451. doi:10.1002/pssc.201300761.

[106] S. Bonetta, S. Bonetta, F. Motta, A. Strini, E. Carraro, "Photocatalytic bacterial inactivation by TiO_2-coated surfaces", *AMB Express: Springer Open Journal*. 3 (2013) 59. doi:10.1186/2191-0855-3-59.

[107] W. Wang, G. Huang, J.C. Yu, P.K. Wong, "Advances in photocatalytic disinfection of bacteria: Development of photocatalysts and mechanisms", *Journal of Environmental Sciences*. 34 (2015) 232–247. doi:10.1016/j.jes.2015.05.003.

Appendix A

Figure A.1 shows the energy dispersive X-Ray spectroscopy analyses of the pristine papers, *i.e.* Whatman, office and hospital papers. **Figure A.2** depicts the ZnO and TiO_2 nanostructures, as well as the ZnO/TiO_2 heterostructure grown on the different paper-based substrates.

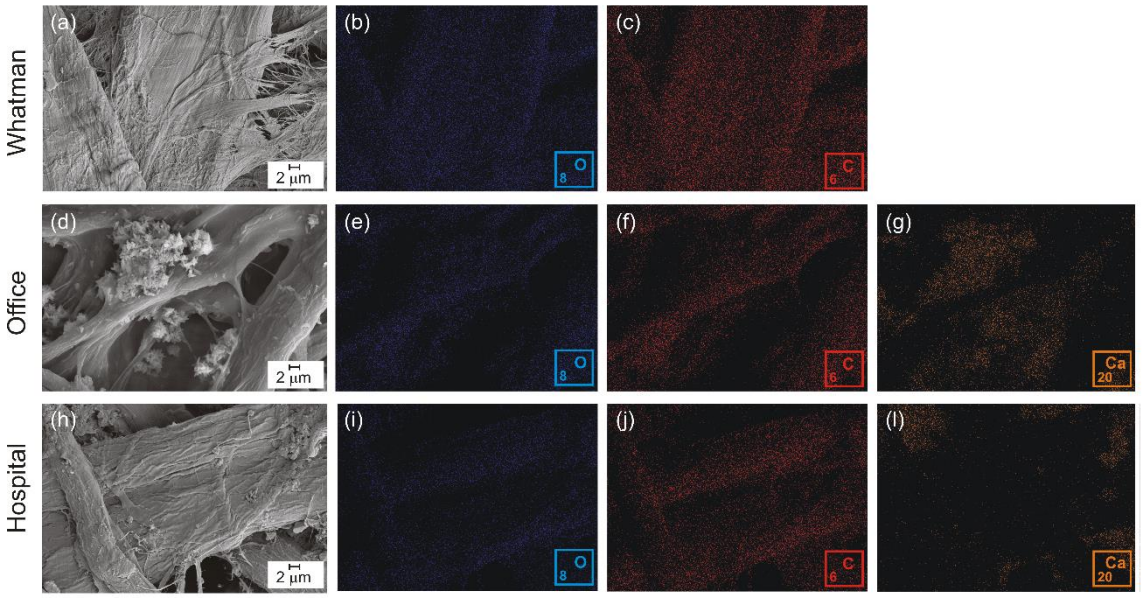

Figure A.1 – SEM images of the pristine papers (a) Whatman, (d) office and (h) hospital. The corresponding EDS maps of O (b, e and f), C (c, f and j), Ca (g and l). Minimal amounts of Al and Si were detected on hospital paper, appearing as clusters.

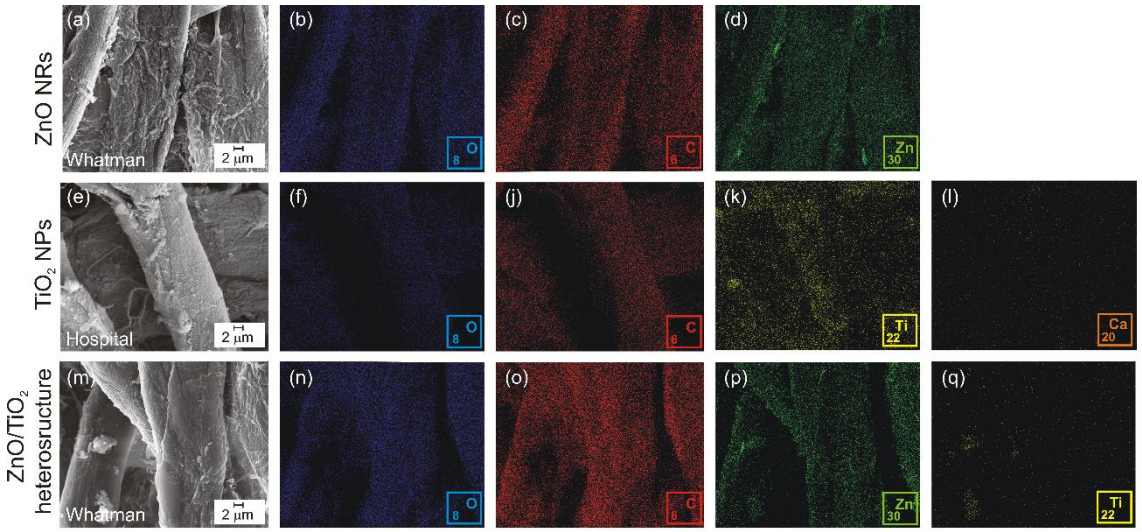

Figure A.2 – SEM images of the materials after microwave synthesis (a) ZnO NRs grown on Whatman paper, (e) TiO_2 nanoparticles (NPs) grown on hospital paper for 15 min (1 M) and (m) ZnO/TiO_2 heterostructure (ZnO NRs with TiO_2 NPs (25 mM-15 min)) grown on Whatman paper. The corresponding EDS maps of O (b, f and n), C (c, j and o), Ti (k and q), Zn (d and p) and Ca (l). Minimal amounts of Al and Si were detected on hospital paper, appearing as clusters.

Figure A.3 shows the Raman spectroscopy measurements of the ZnO and TiO_2 nanostructures grown on Whatman paper and the paper spectrum itself. The intense peaks coming from the substrate obscured the ZnO and TiO_2 signals.

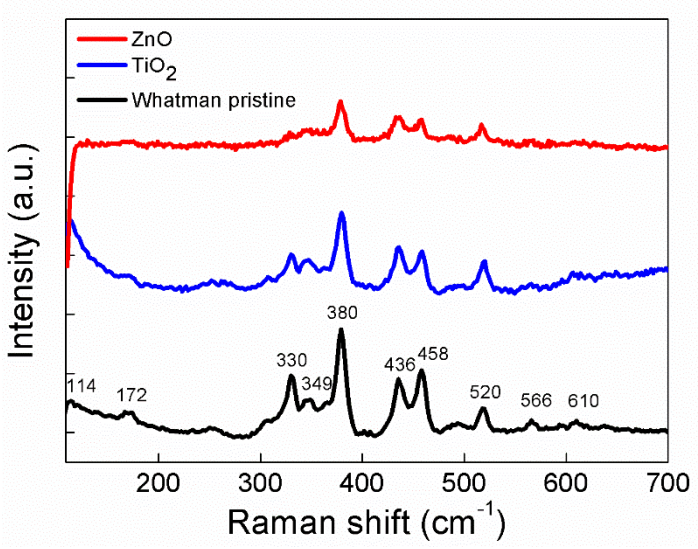

Figure A.3 – Raman spectra of the ZnO and TiO_2 nanostructures grown on Whatman paper under microwave irradiation. The pristine Whatman paper is also presented.

Figure A.4 shows the XRD measurements of the TiO_2 powder formed during the ZnO/TiO_2 heterostructure microwave synthesis. The TiO_2 synthesis was carried out without any acid.

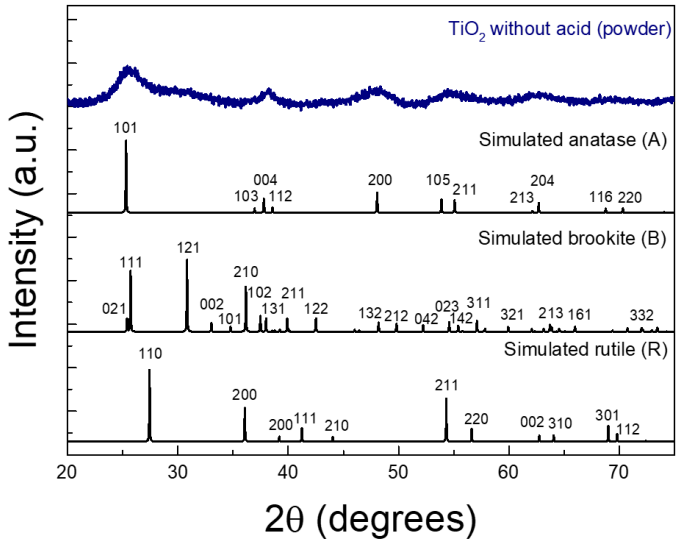

Figure A.4 – XRD measurements of the TiO_2 powder synthesized without the use of any acid during synthesis.

Appendix B

B1. RF sputtering conditions

In order to grow the ZnO nanostructures, the ZnO seed layer was deposited by radio frequency (RF) sputtering with Argon (Ar), at room temperature. A ceramic oxide target of ZnO with a purity of 99.99% was used for the deposition. For the depositions, the chamber was evacuated to a base pressure of 10^{-6} mbar. A shutter between the substrate and the target enabled the protection of the targets from cross contamination. For the deposition of ZnO seed layer, it was used a power of 50 W and a deposition pressure of 4×10^{-3} mbar. The distance between the target and substrate was fixed at 15 cm. The deposition was carried out for 90 minutes allowing the formation of ~ 200 nm ZnO layer [9].

B2. Photocatalytic activity

The paper-based materials were placed on the bottom of the reaction recipient and for each experiment, 50 mL of the rhodamine B solution (5 mg/L) was stirred for 30 min in the dark to establish absorption–desorption equilibrium.

B3. Diffuse reflectance measurements

Room temperature diffuse reflectance measurements to obtain the optical bandgap were performed using a Perkin Elmer lambda 950 UV/VIS/NIR spectrophotometer with a diffuse reflectance module (150 mm diameter integrating sphere, internally coated with Spectralon). The calibration of the system was achieved by using a standard reflector sample (reflectance, R = 1.00 from Spectralon disk). The reflectance (R) was obtained from 250 to 800 nm.